Forschungszentrum Karlsruhe
in der Helmholtz-Gemeinschaft

Wissenschaftliche Berichte
FZKA 7081

Model to Simulate the Interaction between Boron Carbide and Steam or Air at high Temperature

E.A. Garcia

Institut für Materialforschung

Programm Nukleare Sicherheitsforschung

März 2005

Forschungszentrum Karlsruhe
in der Helmholtz-Gemeinschaft

Wissenschaftliche Berichte
FZKA 7081

Model to Simulate the Interaction between Boron Carbide and Steam or Air at high Temperature

Eduardo A. García*

Institut für Materialforschung
Programm Nukleare Sicherheitsforschung

*Present address:
Avda. Elcano 3316 Piso 12 “A”
1426 Buenos Aires, Argentina
e-mail: anhinga_a@hotmail.com

Forschungszentrum Karlsruhe GmbH, Karlsruhe
2005

Impressum der Print-Ausgabe:

Als Manuskript gedruckt

Forschungszentrum Karlsruhe GmbH
Postfach 3640, 76021 Karlsruhe

Mitglied der Hermann von Helmholtz-Gemeinschaft
Deutscher Forschungszentren (HGF)

ISSN 0947-8620

urn:nbn:de:0005-070818

Zusammenfassung

Modellierung der Wechselwirkung zwischen Borkarbid und Dampf oder Luft bei hohen Temperaturen.

Die Oxidation von Borkarbid in Wasserdampf bzw. Luft wurde in den letzten Jahren am Institut für Materialforschung des Forschungszentrum Karlsruhe intensiv untersucht. Es steht nun ein umfangreicher Datensatz für die Modellierung zur Verfügung.

In diesem Bericht wird ein Modell zur Beschreibung der experimentellen Ergebnisse vorgeschlagen, das auf der Diffusion von Sauerstoff durch eine oberflächliche flüssige Boroxidschicht sowie der Reaktion zwischen B_2O_3 und Dampf unter Bildung flüchtiger Reaktionsprodukte basiert. Mit diesem Modell kann sowohl die Oxidation von B_4C in Dampf als auch in Luft beschrieben werden. Die Oxidationskinetik ist dabei abhängig von Temperatur und Dampfpartialdruck.

Der Einfluss der Porosität der B_4C Proben wurde untersucht.

Da die Lösung der Diffusionsgleichungen viel Rechenzeit benötigt, wurde außerdem eine vereinfachte Korrelation vorgeschlagen, die in SFD Codes eingebaut werden kann.

Mit dem entwickelten Modell konnten verschiedene isotherme und transiente Experimente in der BOX-Anlage sowie thermogravimetrische Tests unter verschiedenen Atmosphären erfolgreich nachgerechnet werden.

Abstract

The oxidation of boron carbide in steam or air was recently extensively studied especially in Forschungszentrum Karlsruhe, Institut für Materialforschung. An important data set is available for the interaction modelling.

An oxygen diffusion model through the superficial liquid boron oxide formed on the boron carbide external surface associated to a superficial reaction between the liquid boron oxide and steam is proposed to simulate the experimental kinetics from BOX rig and thermogravimetric tests on the interaction between steam and boron carbide at a temperature range 800°C to 1400°C. The oxygen diffusion model will be also useful to simulate interaction between boron carbide and $Ar+O_2$ (air simulation) atmosphere when the steam pressure becomes zero.

From the analysis of BOX rig experimental kinetics of non-condensable (H_2, CO_2, CO and CH_4) gases we propose an oxygen diffusion model through the liquid boron oxide and a "steam/liquid boron oxide" superficial reaction that generates condensable (boric acids) and non-condensable gases in two interfaces, the interfaces "gas/liquid boron oxide" and "liquid boron oxide/boron carbide". The superficial reaction is dependent on temperature and steam pressure. A specific analysis is devoted to samples with porosity in comparison to samples without or with very low porosity.

As the calculation of diffusion equation involves extra computing time, we propose a simplified equation particularly useful for big codes.

We prove that the proposed model is able to simulate the H_2, CO_2, CO and CH_4 generation in the case of BOX rig tests under Ar+Steam atmosphere during different experimental conditions like isothermal tests, transient temperature tests and transient steam pressure tests or in the case of thermogravimetric experiments under Ar+Steam and under $Ar+O_2$ atmosphere in different isothermal conditions. The model is also able to calculate the quantity of total condensable gases but for the moment it is not possible to check with any experimental result.

Contens

List of Figures

List of Tables

1. Introduction

The objective of the present investigation is to propose a simple model to simulate the interaction between Boron Carbide, B_4C, with $Ar+H_2O$ (Steam) or $Ar+O_2$ atmosphere at high temperature. Two experiments have recently been performed in IMF-I and IMF-III at FZK, the BOX rig test [1] and the Thermogravimetric test [2] respectively. These two experiences are the most recent. The BOX rig test was especially innovative because it gives us the possibility to analyse the evolution of each non-condensable gas from the sample. Some of the Safety Analysis Codes has limited simulations for B_4C oxidation and H_2 prediction. However, not all of them calculate the CO and CO_2 production able to affect the volatile fission products chemistry in the circuits*.

Two models have recently been proposed to describe this interaction. The first one, IBRAE model [3] §4.2, proposes a surface reaction kinetics and mass transport in the gas phase near the sample as a rate determining process, we will later consider this hypothesis that is the model bases in §0 where we show that this assumption is not correct under the BOX rig experimental conditions. The second one (FZK BORCA model) [3] §4.1 is a semi-empirical model where different diffusion processes contribute to the formation of oxide films on B_4C. It appears that the rate determining process is the gaseous species, especially boric acid by Ar/steam fluid and it proves, as the first model does, that the flow conditions in the coolant channel are decisive for the oxidation rate. Our consideration on §0 is also applicable to this second model. A third treatment is essentially an analysis and evaluation of the thermogravimetric results [3] but it does not include BOX rig analysis. We are in coincidence with the comments in thermogravimetry except when flow rate is considered as an important variable.

The aim of the present study is to propose a new model on oxidation of B_4C during the interaction with steam and air reflecting the new mentioned experiments and to give a model able to explain the kinetics of each non-condensable gas at constant and variable steam pressure. It is also able to simulate simultaneously temperature transient or both temperature transient and steam pressure transient.

Up to now simple and rapid calculations are commonly used in Safety Analysis Codes, in despite of the errors introduced especially in quench process. Therefore, we will propose a correlation for the B_4C oxidation in steam.

2. Overview of experiments

The BOX Rig [1] consists, Fig.1, in a reaction chamber where is placed the sample of B_4C over a support of Y_2O_3 able to be heated up to 1700°C under different atmospheres. Argon is commonly used with a flow rate of 50 l/h plus steam up to 70 g/h. Three types of B_4C pellet samples were tested named FRA (FRAMATOME), COD (CODEX), ESK and ESK powder. Details of geometry, weight, density, surface, volume, specific surface porosity and supplier are given in reference [1] Table 2 and the list of impurities in Table 3. The gas supply system consists of two gas flow controllers, one liquid flow controller and a so-called controlled

* B. Adroguer et al. "Synthesis on plant calculation (D35), Final COLOSS report: Part 2". SAM-COLOSS-P080. IRSN/DRS/SEMAR 03/30. June 2003.

evaporator mixer unit (CEM). The off-gas analysis was performed by a quadrupole mass spectrometer.

The essential results of isothermal experiments on B_4C oxidation in the BOX rig are summarised in Table A2, ref. [1]. It consists of 39 tests distributed: 25 FRA, 8 ESK, 4 COD and 2 ESK powder samples. The temperature range was in general from 800°C to 1400°C at steps of 200°C. Four FRA sample exceptions: two at 900°C and two at 1100°C. The steam injection was of 3 and 30 g/h with a carrier Ar gas of 50 l/h.

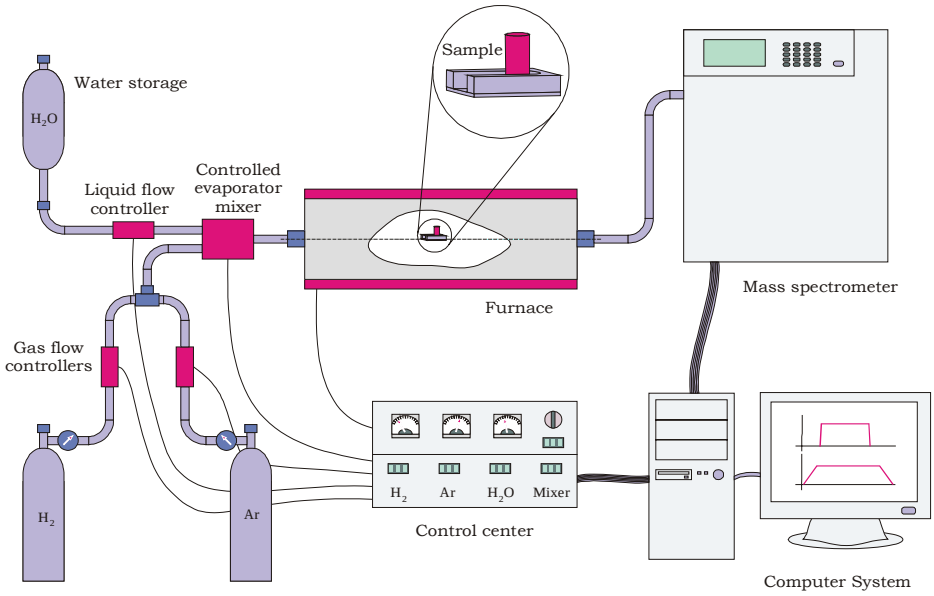

Fig. 1: BOX Rig for the investigation of the oxidation kinetics of B_4C, after ref. [1].

Three experiments were performed with one gas variable injection rate and the others constants: Ar 10-100 ln/h, steam 5-70 g/h and H_2 0-90 ln/h. The sample support was improved during the first tests. For quantitative analysis is better to choose the test performed with the “New sample support”. The quantitative record of each non-condensable gas as a function of time is possible thanks to this innovative method.

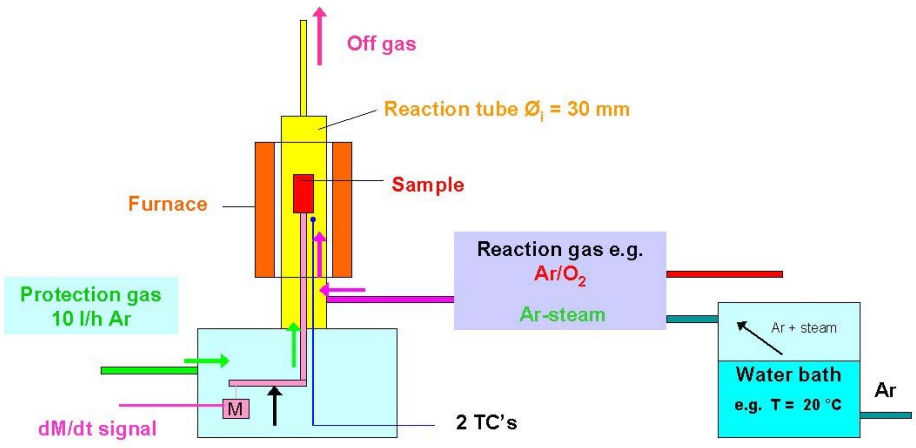

Fig. 2: Schematic view of TG unit with gas supply.

3. Summary of Chemical Reactions

The previous and the recent experimental results (BOX, TG) show that the B_2O_3(l) is a liquid protective layer formed from the oxidation of B_4C(s) during the interaction with pure oxygen and with steam. In the first case the TG result produces a parabolic kinetics and in the second case an important generation of H_2 (g) accompanied of CO_2 (g), CO (g), CH_4 (g), H_3BO_3 (g), HBO_2 (g) is measured and B_2O_3 (l) is detected over the surface of the B_4C(s) according to the following reactions:

$$B_4C + 7H_2O(g) \rightarrow 2B_2O_3(l) + CO(g) + 7H_2(g) \quad (1)$$

$$B_4C + 8H_2O(g) \rightarrow 2B_2O_3(l) + CO_2(g) + 8H_2(g) \quad (2)$$

$$B_4C + 6H_2O(g) \rightarrow 2B_2O_3(l) + CH_4(g) + 4H_2(g) \quad (3)$$

and

$$B_2O_3\,(l) \rightarrow B_2O_3\,(g) \quad \text{direct evaporation at high temperatures: } T>1400°C \quad (4)$$

$$B_2O_3(l) + 3H_2O(g) \rightarrow 2H_3BO_3(g) \quad \text{at low temperature: } 800°C<T<1500°C \quad (5)$$

$$B_2O_3(l) + H_2O(g) \rightarrow 2HBO_2(g) \quad \text{at low temperature: } 800°C<T<1500°C \quad (6)$$

The interaction between B_4C and steam produces four non-condensable gases H_2, CO, CO_2 and CH_4 and B_2O_3 liquid on the B_4C surface, eq. (1) to (3). The reaction between B_2O_3 and steam generates two condensable gases, boric acids eq. (5) and (6) and also direct evaporation at high temperature eq. (4). The B_4C reacts also with $Ar+O_2$ (to simulate the air) to form B_2O_3 liquid on the B_4C surface and two non-condensable gases CO and CO_2.

The thermo-chemical equilibrium calculations were performed in ref. [1] §6 of 1 B_4C and 10 H_2O as a function of temperature using the equiTherm 5.0 software at the built-in Barin database for pure substances. It shows that for the temperature range of BOX rig and TG test, 800°C to 1400°C, the four non condensable gases have constant behaviour, 7 mole for H_2, 1 mole for CO, between 0.3 and 0.1 mole for CO_2 and a significant CH_4 production is only obtained at low temperatures (<700°C) outside of BOX rig and TG temperature test. The CH_4 production is interesting because of its potential influence on the iodine fission products chemistry. The CH_4 could be generated at low temperature by the interaction of CO and CO_2 with water, and then the production of these two non-condensable gases becomes also important[*].

In order to propose a simple model to simulate the interaction between B_4C and steam or air we will start to analyse the BOX Rig experimental results. We will later try to apply the model with some parameters already defined in the BOX Rig to the TG test results in steam and air simulated by $Ar+O_2$.

[*] B. Adroguer et al. "Synthesis on plant calculation (D35), Final COLOSS report: Part 2". SAM-COLOSS-P080. IRSN/DRS/SEMAR 03/30. June 2003.

4. Analysis of BOX Rig Experimental Results.

4.1 The different behaviour of the species generated as a function of time.

4.1.1 The non condensable gases

We intend to analyse the BOX results obtained at constant temperature to elucidate in what interface each species are generated. The Fig. 3 and Fig. 4 show the rate of H_2(g) in comparison with the rates of CO(g), CO_2(g) and CH_4(g). It is clear from these Figures that H_2, CO and CH_4 have a similar behaviour as a function of time. In the case of 800°C and 1000°C and for steam at 3 and 30 g/h this behaviour is evident because the three mentioned molecules have a peak for small times, an then, they have a tendency to stabilise. On the contrary the CO_2 has no peak, growing continuously from the beginning of the experiment up to the end, showing also a tendency to stabilise for longer times.

In the experiments at 1200°C and 1400°C and steam at 3 g/h these characteristics persist but it is not clear for 1200°C and 1400°C and steam at 30 g/h.

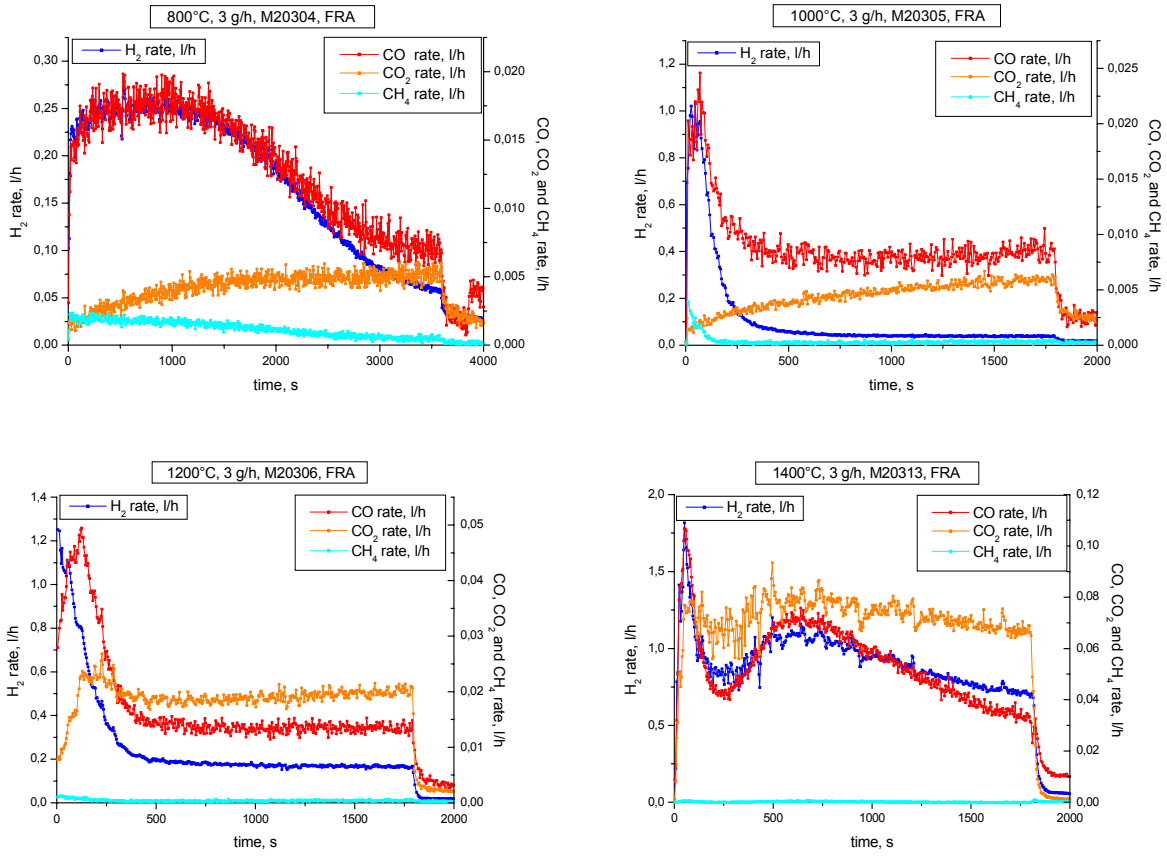

Fig. 3: BOX Rig results of FRAMATOM (FRA) samples at different temperatures: 800°C, 1000°C, 1200°C and 1400°C. At low steam partial pressure, 3 g/h. In the left Y: H_2 rate, l/h and in the right Y: CO, CO_2 and CH_4 rate in l/h as a function of time in seconds. The M number corresponds to BOX rig experimental denomination [1].

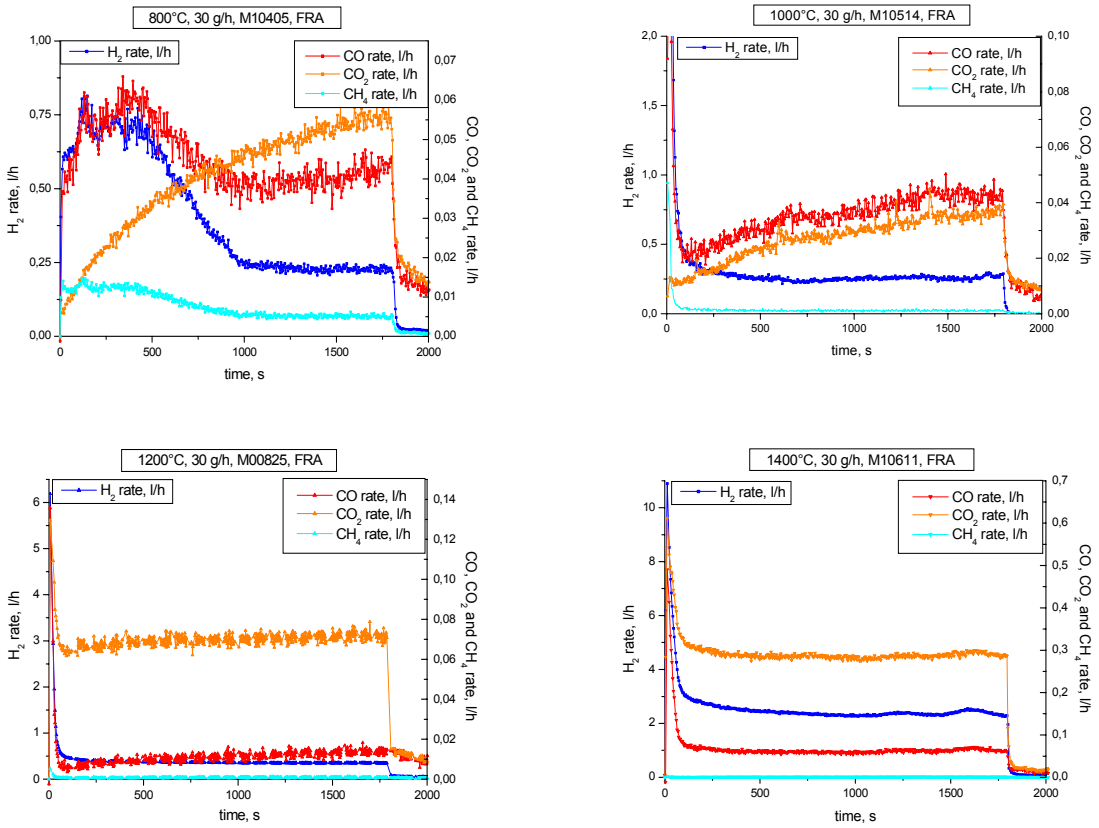

Fig. 4: BOX Rig results of FRAMATOM (FRA) samples at different temperatures: 800°C, 1000°C, 1200°C and 1400°C. At steam partial pressure, 30 g/h. In the left Y: H_2 rate, l/h and in the right Y: CO, CO_2 and CH_4 rate in l/h as a function of time in seconds. The M number corresponds to BOX rig experimental denomination [1].

To show that this is still valid, we consider the total gas detected involving Carbon: $CO+CO_2+CH_4$ and we represent the percent of each component as a function of time, Fig. 5 The tendency showed in the previous analysis persists in these experiments; the CO has in all the cases a peak at the beginning of the kinetics. On the contrary, the CO_2 has no peak and grows from low values at the start up to stabilise in a value for longer times like CO.

As CH_4 has very low values, a representation in logarithmic scale to evaluate its behaviour, Fig. 6, is necessary.

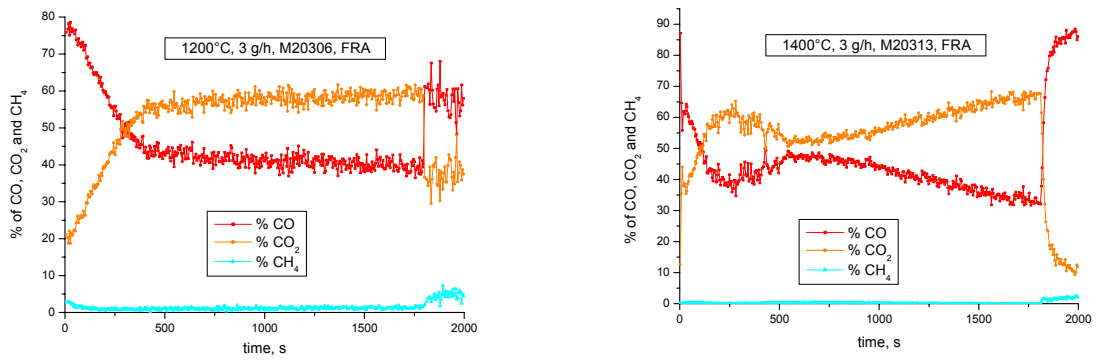

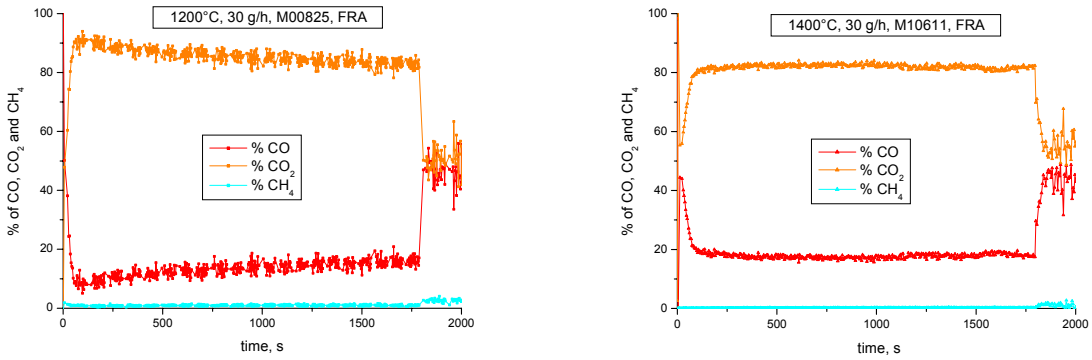

Fig. 5: BOX Rig results of FRAMATOM (FRA) samples at different temperatures: 1200°C and 1400°C. At steam partial pressure, 3 g/h and 30 g/h. Percent of CO, CO_2 and CH_4 as a function of time in seconds. The M number corresponds to BOX rig experimental denomination [1].

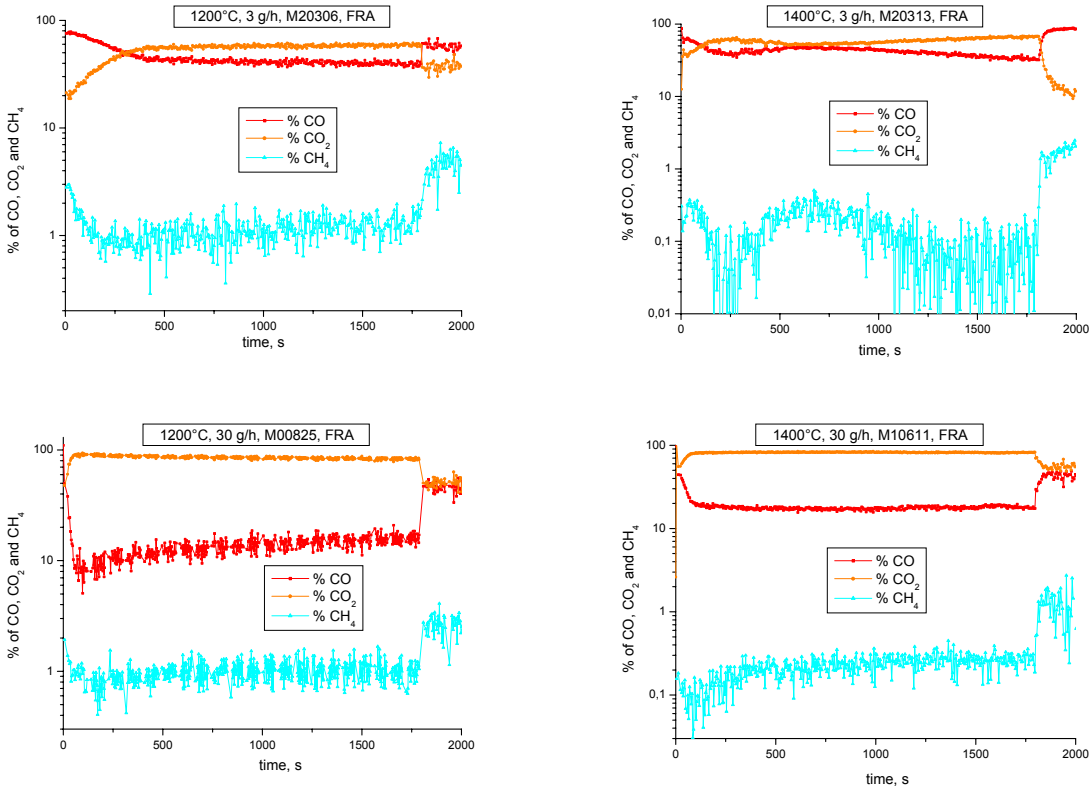

Fig. 6: BOX Rig results of FRAMATOM (FRA) samples at different temperatures: 1200°C and 1400°C. At steam partial pressure, 3 g/h and 30 g/h. Decimal logarithms of percent of CO, CO_2 and CH_4 as a function of time in seconds. The M number corresponds to BOX rig experimental denomination [1].

In Fig.6 CH_4 has similar comportment to CO and H_2 as we showed before and different to CO_2.

We conclude that H_2, CO and CH_4 are generated in a similar way or place during the reaction and different to CO_2.

4.1.2 The condensable gases

The condensable gases were also measured by the MS[1]. The condensable gases detected were: $H^{10}BO_2$ mass 43, $H^{11}BO_2$ mass 44, $H_3{}^{10}BO_3$ mass 61, $H_3{}^{11}BO_3$ mass 62 and a signal in mass 45 were not identified. Fig 7 shows as an example two temperatures at steam 30 g/h of condensable gases with the percents of non-condensable gases that contains Carbon. At low temperatures the condensable gases has the same behaviour than CO_2 but at high temperatures the $H^{11}BO_2$ (amu 44) presents a peak in surface.

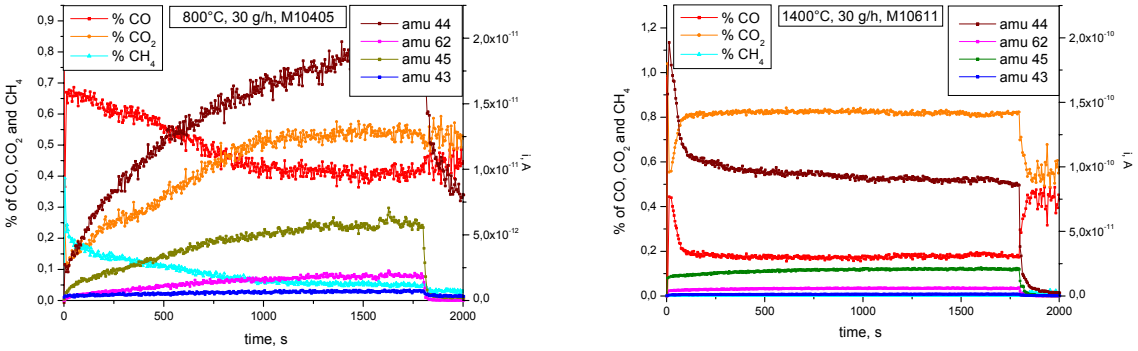

Fig. 7: Comparison of MS results of condensable and non-condensable gases between low and high temperature and steam 30 g/h. The M number corresponds to BOX rig experimental denomination [1].

A similar behaviour is observed in Fig. 8 in the case of an identical comparison for steam at 3 g/h. The fact that CO_2 (amu 28 and 44) shows a similar behaviour at low temperatures like all condensable gases could induce us to think that the conclusion of the precedent paragraph could be incorrect due that CO_2 is partially determinate by the amu 44. The result at high temperature shows that the separation introduced during the measurement of CO_2 (amu 28 and 44) and $H^{11}BO_2$ (amu 44) is satisfactory. The others components, all related to boric acid, $H_3{}^{11}BO_3$ (amu 62), $H^{10}BO_2$ (amu 43) and the non-identified (amu 45) have the same behaviour at high and low temperatures.

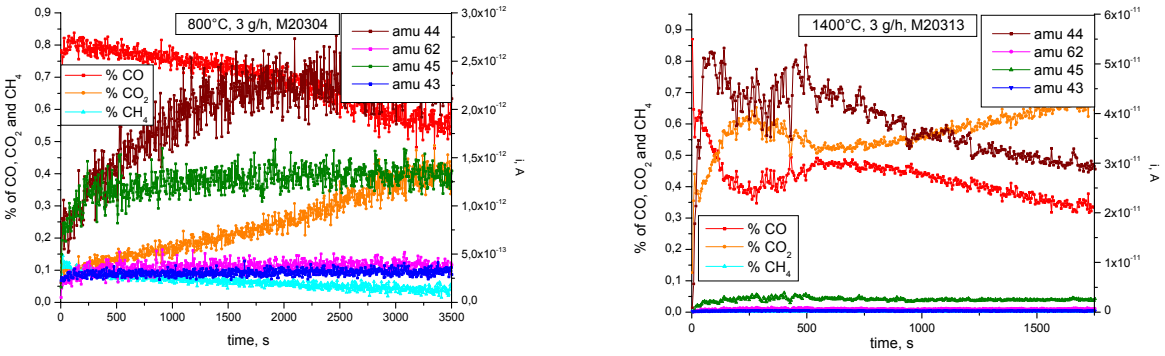

Fig. 8: Comparison of MS results of condensable and non-condensable gases between low and high temperature and steam 3 g/h. The noise is consequence of very low signals level. The M number corresponds to BOX rig experimental denomination [1].

4.2 The dependence on gas dynamic conditions

During the BOX rig test experiments [1] it has been pointed out that the support specimen has an important influence on the results. “The pellets showed an axially non homogeneous oxidation due to the non homogeneous steam flow along the specimen. This was solved by sawing off the wall of the alumina boat direct to the steam flow, showed in Fig. 3”, reference [1]. In the recent final analysis report [3] §2.2, about dependence on gas dynamic conditions, appears the difference between two spectra, Fig. 4. “In the first test specimens were kept in a normal high board alumina boat in the reaction tube. The pellet showed an axially non-homogeneous oxidation due to the non-homogeneous steam flow around the specimen. In the subsequent test the sample support was changed. As a result of this specimen support improvement, steam access to the pellet enhanced and hydrogen production rate increase more than two times”.

We considered that this difference could be due to the fact that the sample surface exposed to the gas in the case of the alumina boat with the sawing wall is bigger than the sample surface exposed with an original alumina boat without the yttria disc separator. The reason is that the Ar has around twice density than the steam. At the beginning of the experiment the original alumina boat without the yttria disc separator is full of Ar, when the Ar+steam is introduced at 50 l/h the Ar present in the original alumina boat protects the sample and only the upper part of the sample reacts as was observed during the first experiments (Fig. 19 ref.[1]). The upper part of the sample that was exposed was 0.44 cm over a total sample high of 1.4 cm in the case of original alumina boat support without the yttria disc separator, Fig. 9 Only under geometrical considerations the 31% of the upper part of the sample will react in the first moment with steam, with matches with Fig. 19 ref. [1] in the case of 800°C and 1200°C. The grey zone matches with about the 31% of the high part of the sample. This area has also a smaller diameter than the lower part of the sample. This gives us the possibility to explain this non-uniform reaction on the sample surface without the necessity to use the reference of the different speed of gases in the top of the sample with respect to the bottom.

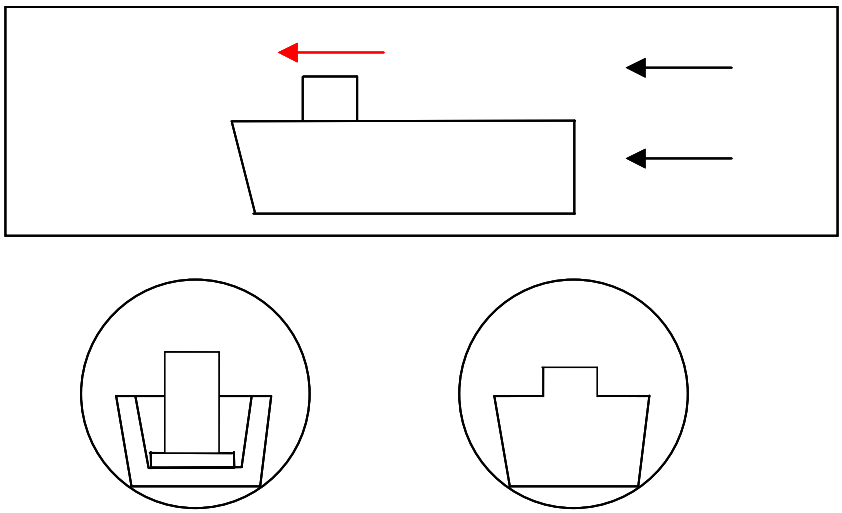

Fig. 9: In the upper part we show a section of the reaction tube with the alumina boat and the sample. In the lower part two sections, the left section shows the sample over the Yttria disc in a open alumina boat, the right section shows the section of a original alumina boat with a sample.

The test number M10126 performed at variable Ar flow rate 50, 10, 30, 50, 70, 90 and 100 l/h and constant steam input of 30 g/h is compared with an experiment at 1200°C and constant steam input of 30 g/h, showed in Fig. 10 a.

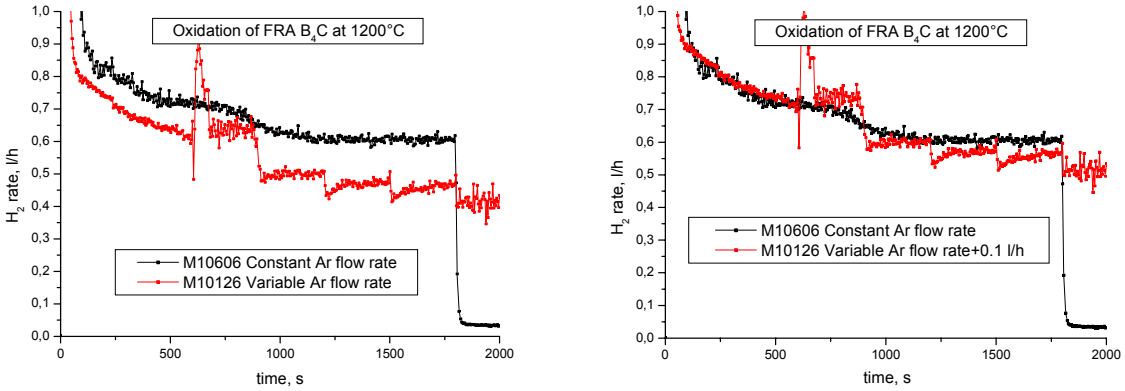

a) b)

Fig.10: a) Comparison between two tests with steam flow of 30 g/h, both at 1200°C. The test M10606 with constant Ar flow 50 l/h and the test M10126 with variable Ar flow from 10 to 100 l/h. b) We add 0.1 l/h in order to produce a coincidence in the first 500s, where the experiments have identical characteristics. The M number corresponds to BOX rig experimental denomination [1].

We observe that the differences between both experiments are not significant for the difference of gas speed proposed. During the first 500 seconds both experiences have the same experimental conditions, so they would be identical. The difference could be attributed to difference in porosity and/or difference on contamination inside the porosity.

In order to show a better comparison and to transform the results of the first 500 seconds in a similar result, we add, in Fig. 10b, 0.1 l/h to the experiment M10126 that corresponds to 0.0033 mole/(m^2s) and the results move us to conclude that the different Ar speed (10 to 100 l/h) has no important influence over hydrogen generation. The change produced in the results, Fig. 10b, could be attributed to perturbation produced on the gas input at the moment when the gas flow changes, rather than to the speed of the Ar carrier, almost in the first approach. This was one of the reasons why we prefer a model in which the control speed of the B_4C oxidation reaction is due to oxygen diffusion in the protective liquid oxide layer of B_2O_3 instead of a model, which would consider a reaction speed change due to Ar gas carrier speed. The reaction between B_2O_3 and steam depends only on the steam partial pressure and temperature but not on the speed of reactant atmosphere almost as used for speed during the experiments, Ar speed 10 to 100 l/h. This model will be presented in the next paragraph.

5. Proposed Model

We consider that the steam in contact with B_4C generates a layer of B_2O_3(l) protective scale which limits the diffusion of oxygen through the liquid oxide layer. It is important to observe that some authors [4,5,6] mention, “The Boron and Carbon diffused through the liquid oxide

layer to be oxidized at the external oxide surface to contribute to the growth of oxide layer". Nevertheless, this affirmation is not proved. Over the cleaning surface of B_4C a rapid reaction occurs producing a peak of hydrogen due to a dissociation of H_2O (Steam) on the surface of the $B_2O_3(l)$ and the diffusion of oxygen through the oxide layer up to the interface $B_2O_3(l)/B_4C(s)$ to oxidize the $B_4C(s)$ and to form $B_2O_3(l)$ and liberate the Carbon partially oxidized to CO in this interface. This sharp Hydrogen peak is shown in the most of the BOX tests like in Fig.3. We know from the equations 1-3 that C will form CO_2, CO with the oxygen and CH_4 with the Hydrogen produced as a consequence of steam dissociation at the external interface, gas/$B_2O_3(l)$.

It is clear from Fig.3 and Fig.4 that the H_2 is the gas generated in a biggest quantity and has these general characteristics: a very important sharp peak when a reaction starts and a constant H_2 production for longer times. CO and CH_4 have similar characteristics. It is necessary to say that for 800°C (3 and 30 g/h) and 1400°C (3 g/h) the system is perturbed for the superficial porosity of the samples as was previously mentioned in the BOX Rig test [1].

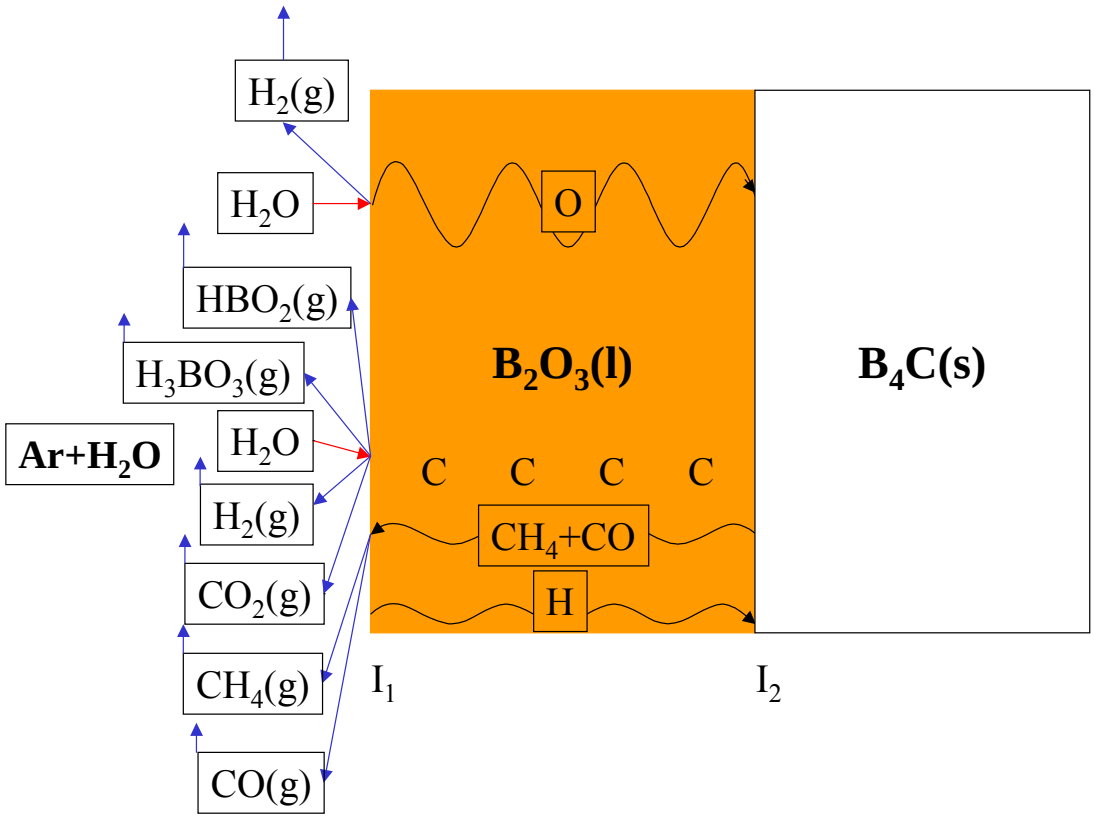

Fig.11: Schema for the Steam/B_4C simulation model.
At the Interface I_1=Ar+H_2O(Steam)/$B_2O_3(l)$, we have the H_2 generation due to dissociation of Steam and the diffusion of Oxygen generated during this dissociation through $B_2O_3(l)$ to oxidize the B_4C at the interface I_2= $B_2O_3(l)/B_4C$.
As a consequence of the oxidation of B_4C in I_2 with the oxygen arrived from I_1 to form $B_2O_3(l)$, Carbon is liberated, a part of them will form CO at I_2 with the oxygen arriving from I_1 and CH_4 with some Hydrogen diffusing from I_1 through $B_2O_3(l)$ up to I_2. Some Carbon are dissolving in the $B_2O_3(l)$ at I_2. During the erosion of $B_2O_3(l)$ at I_1 the Carbon dissolving in it, oxidize to CO_2.

We propose a dissociation of H_2O on the surface of the B_2O_3(l) and the diffusion of oxygen and small quantity of Hydrogen through the oxide layer up to the internal interface B_2O_3(l)/B_4C(s) to oxidize the B_4C(s) generating CO(g) and CH_4(g) and liberating C. Some part of Carbon dissolved in the B_2O_3(l) is oxidized when the steam reacts with B_2O_3(l) at the external interface Ar+H_2O(Steam)/B_2O_3(l).The Carbon is oxidized at CO_2. In this way we are able to understand the different behaviour of these gaseous molecules during the reaction kinetics,§4.1.

Under this hypothesis the Steam/B_4C(s) interaction is schematically shown in Fig. 11. Then, we have H_2 generated at the external interface but according to the necessary quantity of oxygen at the internal interface, I_2. The CO and CH_4 also generated at the internal interface, I_2, and finally the CO_2 at the external interface, I_1.

5.1 The model diffusion equations

In order to have a constant generation of H_2 with oxygen diffusion through a protected oxide, this oxide layer must keep constant for longer times, during steady state. This means the interfaces I_1 and I_2 will travel with the same speed. For short time at the beginning a transient must appear.

We will propose the simplest model able to simulate the BOX Rig and the TG experimental results.

In Fig.12 we have in the coordinates system A an oxide layer, B_2O_3(l), that grows as a consequence of oxidation of B_4C. In principle we suppose that no expansion during the oxidation happened, this means that one cm^3 of B_2O_3 is formed in lieu of one cm^3 of B_4C. We know that this is not the reality of our system but we accept it as a first approach to the problem. It will be then necessary to compensate according to the approximate density the oxide formed.

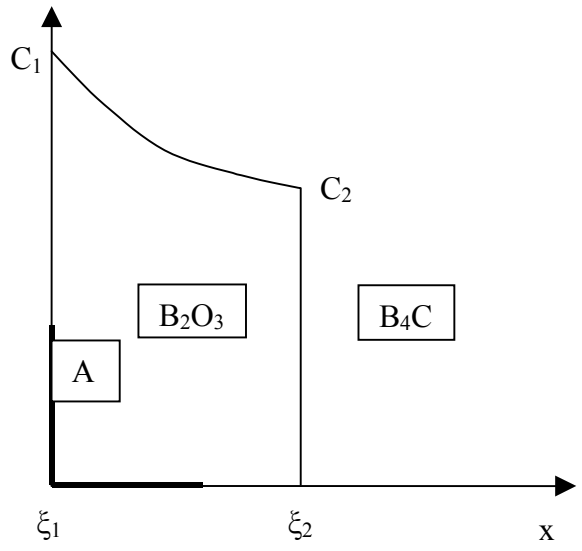

Fig. 12: Schema for the B_4C oxidation in a Ar+O_2 atmosphere

This approach to the problem is due to a lack of knowledge about the parameters of the system. In Fig. 12 for example we are able to calculate C_2 but the value of C_1 that will give the oxygen gradient through the oxide layer is completely unknown as well as the oxygen diffusion coefficient in the oxide and the oxide layer thickness.

The diffusion equations of the model proposed in Fig. 12 are:

The diffusion equation in system A (ξ_1 is fixed to the system A):

$$D\frac{\partial^2 C}{\partial x^2}=\frac{\partial C}{\partial t} \tag{7}$$

and the Stefan equation in system A:

$$-D\frac{\partial C}{\partial x}\Big]_{x=\xi_2}=C_2\,\frac{d\xi_2}{dt} \tag{8}$$

These equations represent the model under the approximation proposed for the oxidation of B_4C in $Ar+O_2$ atmosphere.

When we change the atmosphere to Ar+Steam the steam reacts with the B_2O_3(l), the Steam (H_2O) dissociates at its surface or this surface is able to evaporate especially at high temperatures. This process reduces the thickness of oxide layer of B_2O_3(l) at speed v, where evaporation and reaction are included. This speed v is constant for any time and changes with temperature and partial pressure, $v=v(T, p_{H_2O})$ as a hypothesis of the model. Then, in the system A, the new behaviour of the model proposed in Fig.12, is shown in Fig. 13 The interface that was placed at the origin moves at a constant speed $v=x/t=d\xi_1/dt$, because T and p_{H_2O} are constant.

The interface, ξ_2 will move according to the Stefan equation showed in Fig. 13 This interface will have an equilibrium position at a given distance from the interface ξ_1. The equilibrium position is supposed to be ξ_2. If the interface is displaced to the position ξ_2^+ the slope $-\partial C/\partial x\big]_{\xi_2^+}$ is smaller than $-\partial C/\partial x\big]_{\xi_2}$ then $d\xi_2^+/dt$ will decrease the speed, carrying the interface to the position ξ_2. A similar reaction would happen if the interface is moved at the place ξ_2^- the speed will increase, carrying the interface to the equilibrium position ξ_2.

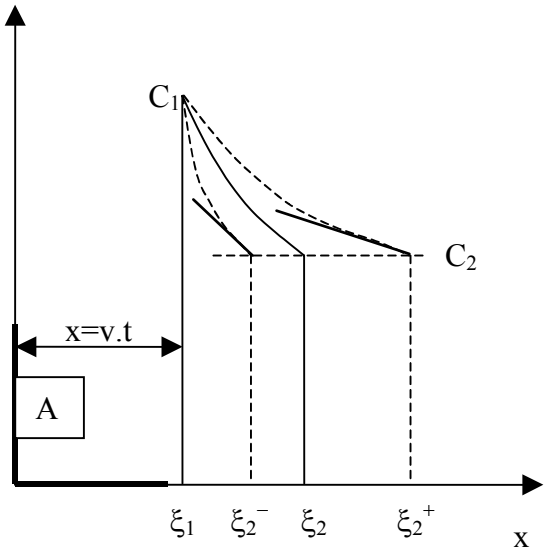

$$\frac{d\xi_2}{dt}=-\frac{D}{C_2}\cdot\frac{\partial C}{\partial x}\Big|_{\xi_2}$$

Fig. 13: Schema of B_4C oxidation in a Ar+Steam atmosphere in system A.

We propose to describe the system of Fig.13 from a coordinate system B fixed to the interface ξ_1 or to the oxide layer. From the coordinate system B the oxide moves with speed -v, from interface ξ_2 to the interface ξ_1. The diffusion equations for the system B, Fig.14, are:

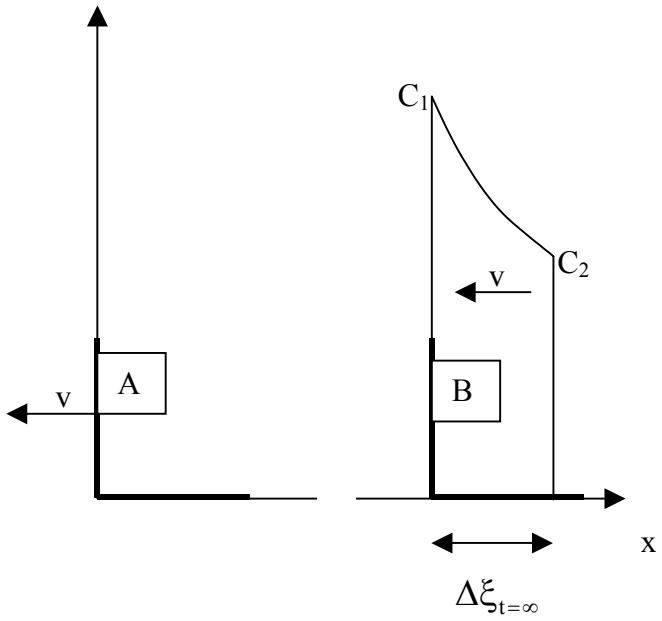

Fig. 14: The same schema of Fig. 13 for the observer placed in the coordinate system B fixed to the oxide layer.

$$D\frac{\partial^2 C}{\partial x^2} - v.\frac{\partial C}{\partial x} = \frac{\partial C}{\partial t} \tag{9}$$

Stationary state in system B:

$$D\frac{\partial^2 C}{\partial x^2} = v.\frac{\partial C}{\partial x} \quad ; \qquad \frac{\partial C}{\partial t} = 0 \quad ; \qquad t = \infty \tag{10}$$

We are able to find the solution for the stationary state with the condition imposed for the model of -v, Fig. 14:

$$\frac{D}{v}.\frac{\partial^2 C}{\partial x^2} = \frac{\partial C}{\partial x} \quad ; \qquad v < 0 \tag{11}$$

The solution is:

$$C = C_1.\exp(-\frac{v}{D}x) \tag{12}$$

When $x = \xi_2 = \Delta\xi_{t=\infty}$, in the system B, C must be equal to C_2, then

$$C_2 = C_1.\exp(-\frac{v}{D}.\Delta\xi_{t=\infty}) \tag{13}$$

We are able to know the oxide layer thickness, that corresponds to the equilibrium position of I_2 related to the moving I_1, as a function of the oxygen diffusion coefficient, D, speed of the ξ_1 interface, v, concentration at the interfaces ξ_1 and ξ_2.

$$\Delta\xi_{t=\infty} = \frac{D}{v}.\ln\left(\left(C_1/C_2\right)\right) \qquad (14)$$

This analytical solution permits us to compare the oxide layer thickness with the one obtained by the numerical solution for longer times.

The Stefan equation for a person standing in system B is the flux arriving at the interface ξ_2 just to compensate the speed of oxide travelling in the contrary sense:

$$F_B = -D.\frac{\partial C}{\partial x}\Big]_{\xi_2} + \vee.C_2 = 0 \qquad \vee < 0 \qquad (15)$$

That is the Stefan equation on Fig. 13, for the stationary conditions $\frac{d\xi_2}{dt} = v$.

6. The Numerical Solution

To know the behaviour of the proposed model as a function of different variables and to simulate experimental results it should be useful to have a numerical solution. We will use a similar code philosophy already developed [7(see appendix)] for this purpose.

The numerical solution gives us the interface position l_1 and l_2 as function of time and the oxygen concentration profile as a function of time and position, when we give the C_1, C_2, $D_O(T)$ and v(T,p) as input.

The numerical solution allows to confirm the previous results, §5.1.

shows the oxide layer thickness as a function of time and also the value for steady state in coincidence with the one obtained by eq. (14).

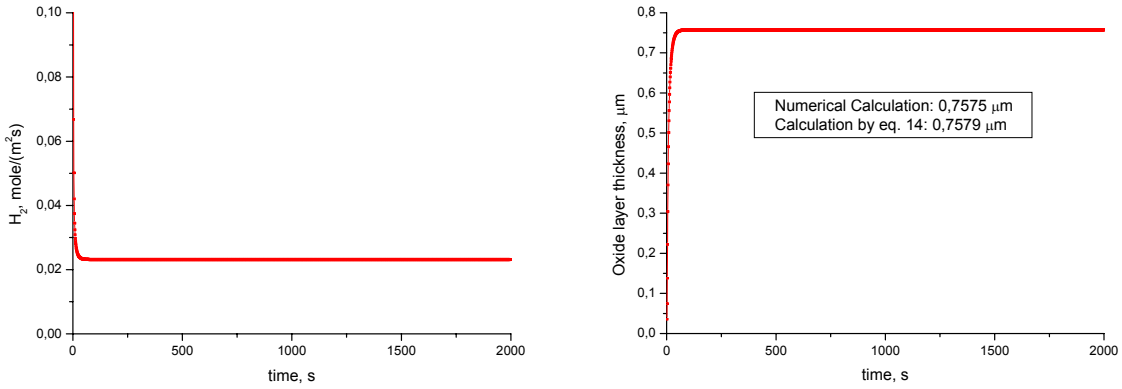

a) b)

Fig. 15: a) Example of hydrogen generation due to numerical calculation. b) The correspondent oxide layer thickness and comparison between numerical calculation and the value given by equation (14).

7. The Calculus of Different Model Parameters

As a result of the solution of diffusion equation eq.(7) and Stefan equation eq.(8) we will obtain the interface positions l_1 and l_2 as a function of time and the oxygen concentration profile for a given set of values, like the concentration at the interfaces (that could be functions of temperature): C_1, C_2, the diffusion coefficient as a function of temperature: D(T) and the erosion speed v, of l_1 as a function of temperature and steam partial pressure: $v=v(T, p_{H_2O})$ and other parameters that reflect the surface state.

7.1 The value of C_2

According to eqs. (1), (2) and (3) and the results of BOX Rig related to the percent of CO, CO_2 and CH_4 we evaluate the average as a function of temperature and pressure and we establish: 85% for CO_2, 14% for CO and 1% for CH_4 as a general rule, because up to now, it is not possible to explain the behaviour of these gases as a function of temperature and time, (see [1] § 5.2.5 Fig. 32 and [3] § 2.3 Fig. 5 and the respective comments).

We don't consider CH_4 because is too small related with the other components.

The equation (2) is the main equation because each mole of B_4C generates: 85% of CO_2, 6 moles of O in the oxide and 14% of one mole of CO. Then:

The molar mass of B_4C: M_{B_4C} = 55.255 g

The molar mass of O: M_O = 15.999 g

ρ_{B_4C} (FRA) = 1.8 g/cm^3

ρ_{B_4C} (ESK) = 2.34 g/cm^3

C_2(FRA)=(6.0+0.14). ρ_{B_4C} (FRA). $M_O.10^3/M_{B_4C}$, mg/cm^3

C_2(ESK)=(6.0+0.14). ρ_{B_4C} (ESK). $M_O.10^3/M_{B_4C}$, mg/cm^3

C_2(FRA) = 3200.0 mg/cm^3

C_2(ESK) = 4160.1mg/cm^3

The necessary oxygen to oxidize the B_4C plus the oxygen to oxidize the CO is similar to the value we obtain if we calculate the necessary oxygen to form B_2O_3 plus the oxygen to oxidize the CO with the hypothesis proposed of no oxide expansion:

The molar mass of B_2O_3 : $M_{B_2O_3}$ = 69.619 g

1 mole of B_4C = M_{B_4C} = 55.255 g → 2 mole of B_2O_3= 2.$M_{B_2O_3}$ = 139.238 g according to the eq. (2), then:

1 M_{B_4C}/ρ_{B_4C} (FRA) = V(B_4C(FRA)) = 30.697 cm^3

1 M_{B_4C}/ρ_{B_4C} (ESK) = V(B_4C(ESK)) = 23.613 cm^3

2. $M_{B_2O_3}$ / V(B_4C(FRA)) = $\rho_{B_2O_3}$ (from B_4C(FRA)) = 4.536 g/cm^3 due to non expansion

2. $M_{B_2O_3}$ / V(B_4C(ESK)) = $\rho_{B_2O_3}$ (from B_4C(ESK)) = 5.897 g/cm^3 due to non expansion

C_2(FRA) = 3. $\rho_{B_2O_3}$ (FRA). M_O.10^3. / $M_{B_2O_3}$ +0.14. ρ_{B_4C} (FRA). M_O. $10^3/M_{B_4C}$, mg/cm^3

C_2(ESK) = 3. $\rho_{B_2O_3}$ (ESK). M_O.10^3. / $M_{B_2O_3}$ +0.14. ρ_{B_4C} (ESK). M_O. $10^3/M_{B_4C}$, mg/cm^3

C_2(FRA) = 3200.2 mg/cm^3

C_2(ESK) = 4160.4 mg/cm^3

7.2 The value of C_1

This value is unknown. We will try a very low value, but it must be bigger than C_2. Nevertheless the $\Delta C = C_1-C_2$ is directly related with the D value. If we increase ΔC or $\ln(C_1/C_2)$ we must decrease D in a similar quantity to obtain the same result and vice-versa.

ΔC = 1.14 mg/cm^3.

7.3 The oxygen diffusion coefficient, D

In the case of the BOX Rig experiment this value has no importance except for the isothermal experiments under variable steam pressure that give us an upper value we will comment later, §9.1.3. On the contrary, it is very important in the TG experiments because of its influence on the oxide layer thickness.

$D_O^{B_2O_3} = D(T) = 2.47\ 10^{-4}\ e^{-9513.8/T}$, cm^2/s, T in °K

The exponential and pre-exponential values are those used during the calculation but they are not related with any physical reason.

The low value used in the exponential factor is related with the fact that it has an influence on the behaviour of oxide layer thickness during steady state. With this value the oxide layer thickness becomes thin for the high and low temperatures considered. We will return later in §7.8.

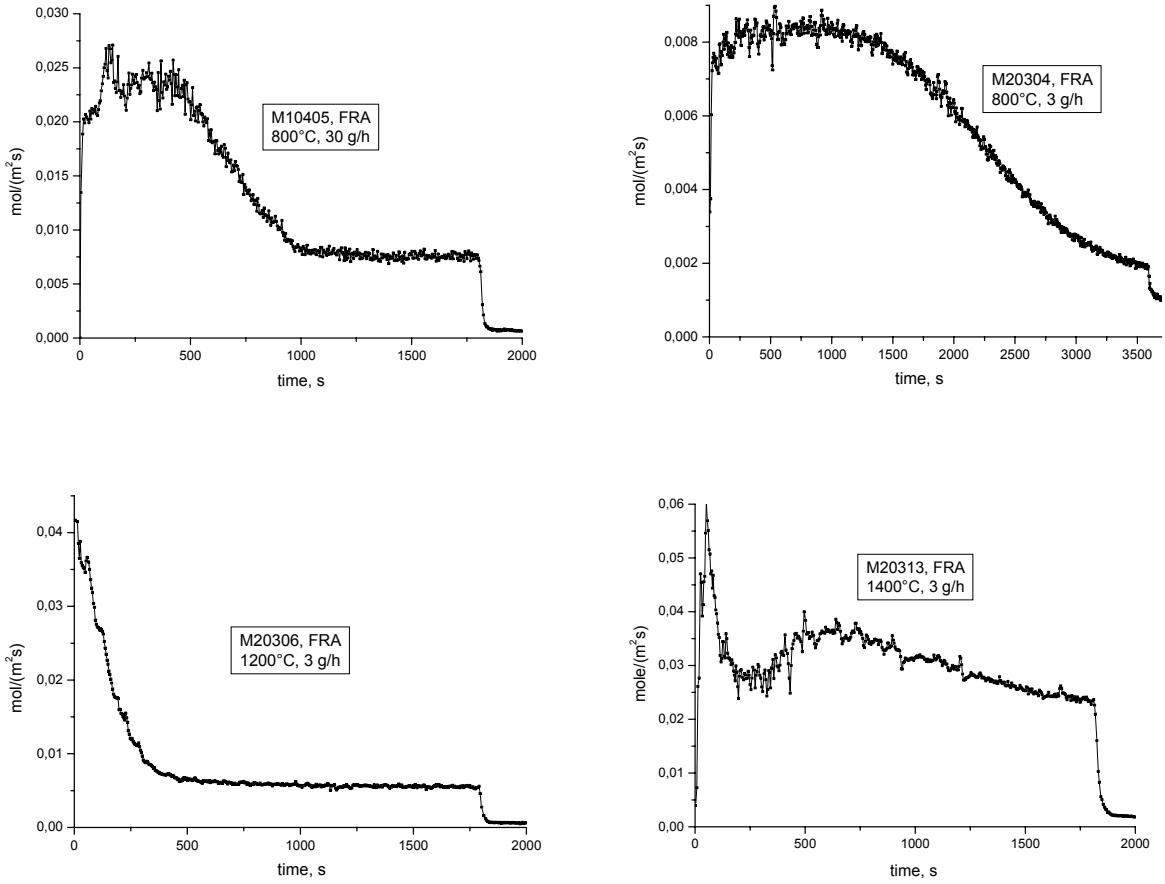

Fig. 16: The four cases in the FRA samples in which an initial peak of extra hydrogen generation appears. The M number corresponds to BOX rig experimental denomination [1].

7.4 The surface porosity

The surface porosity was indicated [1] and [3] as the main factor for the extra hydrogen production at the beginning of the reaction kinetics shown in the Fig.16. These four kinetics in FRA samples show these phenomena. In the case of low temperature, 800°C, for 3 and 30 g/h of steam, the initial peak is very important and extended. Especially in the case of 3 g/h the intensity of the peak is low; the effect is prolonged 3.5 times more than 30 g/h.

For highest temperatures the effect only appears for low steam pressure, 3 g/h and becomes more important and with a special structure at 1400°C: an initial peak and later a second one. This is perhaps due to the surface porosity and the oxide layer thickness and also to a different process taking place as a function of temperature that will we mention in §7.5. Then, an important peak appears at low and at high temperatures and this could be related with the oxide layer thickness. We will return later to this point, §7.8. It is important to say that the model predicts a sharp peak at the beginning of the kinetics when the liquid oxide layer is very thin and grows very fast.

7.4.1 The possible consequences in the oxidation process

As mentioned in the precedent paragraph the average size of the surface porosity and the oxide layer thickness play an important role in the extra hydrogen initial peak.

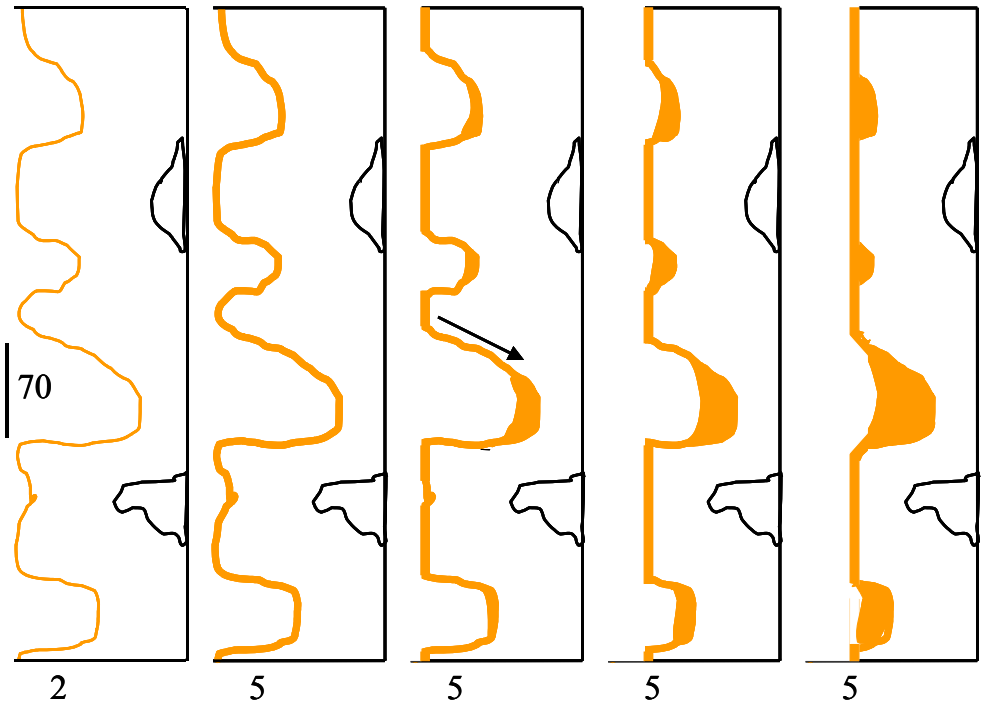

Fig. 17: Growth of a very thin oxide layer during a reaction with steam. The oxide layer thickness (a number in the bottom of each picture) is a fraction of average size porosity.

In Fig.17 we show a possible growth of a very thin oxide layer. The oxide layer we propose has 5 units of thickness and the porosity has about 50 units. We presume a liquid oxide accumulation (see [→] in Fig. 17) at the bottom of the open porosity, that with the time will reduce the effective external surface at I_1, but not the internal surface at I_2.The accumulation could be produced by oxygen starvation in the porosity end and by the reduction of hydrogen production due to the increase of oxide layer. The necessary oxygen to oxidize the B_4C will decrease according to the equation in Fig. 13, in the case that the interface I_2 is in position ξ_2^+. The accumulation of oxide will finally cover the external surface and show an external surface similar to the geometrical one. If the oxide accumulation is not achieved in all over the surface, the oxide layer will have the same thickness and the same effective surface at I_1 and at I_2. They are both bigger than the sample geometrical surface.

In the case of oxide layer thickness grows more than the average size porosity the situation could be that of Fig. 18.

The oxide layer we propose grows up to 81 units of thickness and the porosity has about 70 units. In this case also the external surface at I_1, will approach the sample geometrical surface and the internal surface at I_2, seams to be equal or bigger than the surface at I_2 proposed in Fig. 17.

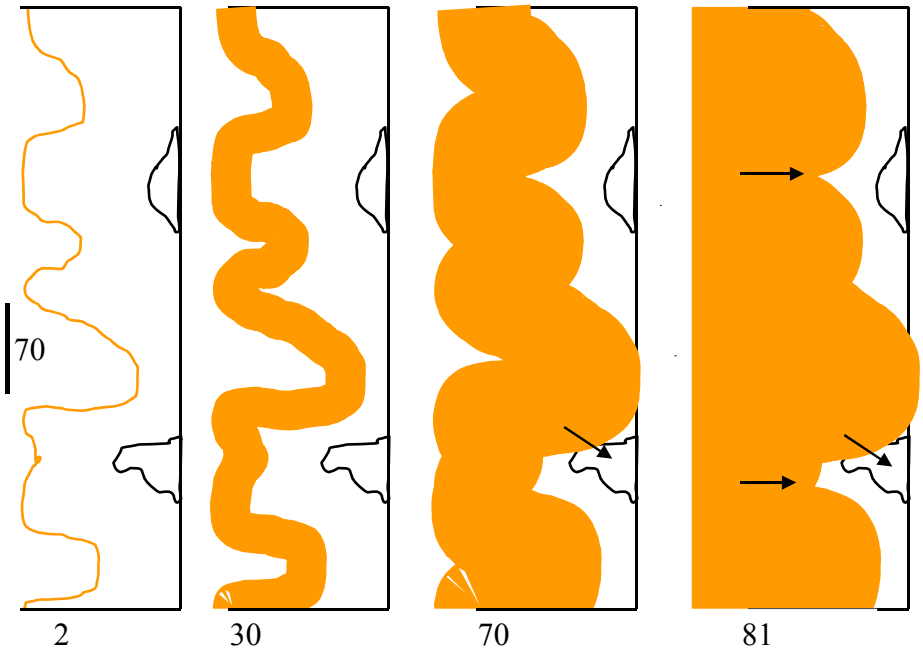

Fig. 18:: Growth of a very thick oxide layer during a reaction with steam. The oxide layer thickness (a number in the bottom of each picture) is the same order of magnitude or bigger than the average size porosity.

7.4.2 The influence on the steady state of FRA samples

We must consider that the steam reaction with FRA samples has the particularity that the internal surface in I_2, is, according to §7.4.1, always bigger than the possible external one in I_1. Because we will take as a reference the set of experiments with the samples ESK in the determination of v(T). We must impose to the experience with bigger porosity like FRA an increase of the effective surface, particularly in the I_2 interface. At the same time we must introduce a correction to simulate the initial hydrogen peak in the cases shown in Fig. 16.

The correction we propose is the simple Gauss function:

$$C_{sup} = C_{sup0} + F_{sup}.\exp(-(t-t_0)^2/(\sigma)^2)$$

Shown in Fig. 19.

The $C_{sup0} \geq 1$, will be used to compensate the permanent surface bigger value at I_2 in the case of FRA samples. This will be considered in the next paragraph.

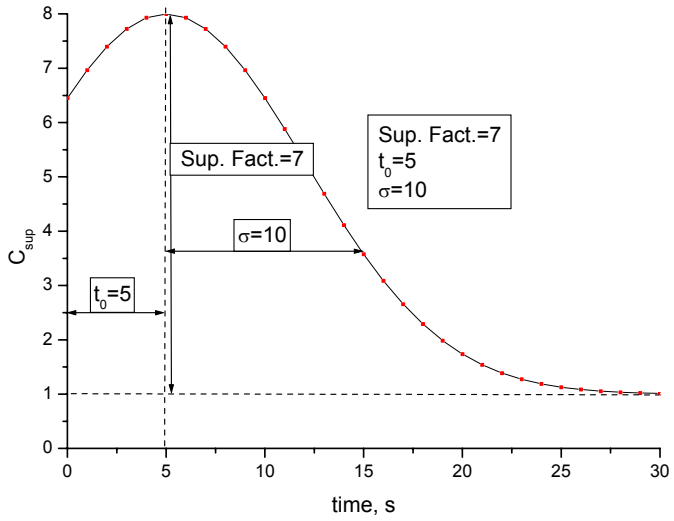

Fig. 19: Generic Gauss function to reproduce the initial hydrogen peak. C_{sup0}=1

7.4.3 The different densities between FRA and ESK samples

It is evident from our model that in the case of FRA samples the quantity of oxygen necessary to oxidize the B_4C will be lower than in the case of ESK samples because:

C_2(FRA) = 3200.2 mg/cm^3 < C_2(ESK) = 4160.4 mg/cm^3, from § 7.1. Then, our model will calculate kinetics of hydrogen in steady state: H_2(ESK) > H_2(FRA). If we observe the general behaviour from BOX Rig experiment (see [1] § 5.2.5 Fig. 31) during steady state, the FRA samples generate more hydrogen than the ESK samples with some exceptions where the release rate can be considered almost equal.

Fig. 20 shows an example of this type, the FRA sample generates more H_2 than the ESK on the contrary the model simulation for FRA sample generates less H_2 than the ESK sample.

In our opinion, these observations reinforce the assertion in § 7.4.1. In the case of FRA samples the surface that corresponds to the I_2 interface is always bigger than the sample geometrical surface. This is just the interface where the quantity of H_2 to be generated is defined according to our proposed model §5.

This is the reason we need a correction in the case of FRA samples to approach the experimental results of BOX rig, a factor that considers a big surface at the interface I_2 regarding the geometrical surface and constant as a function of time, C_{sup0}.

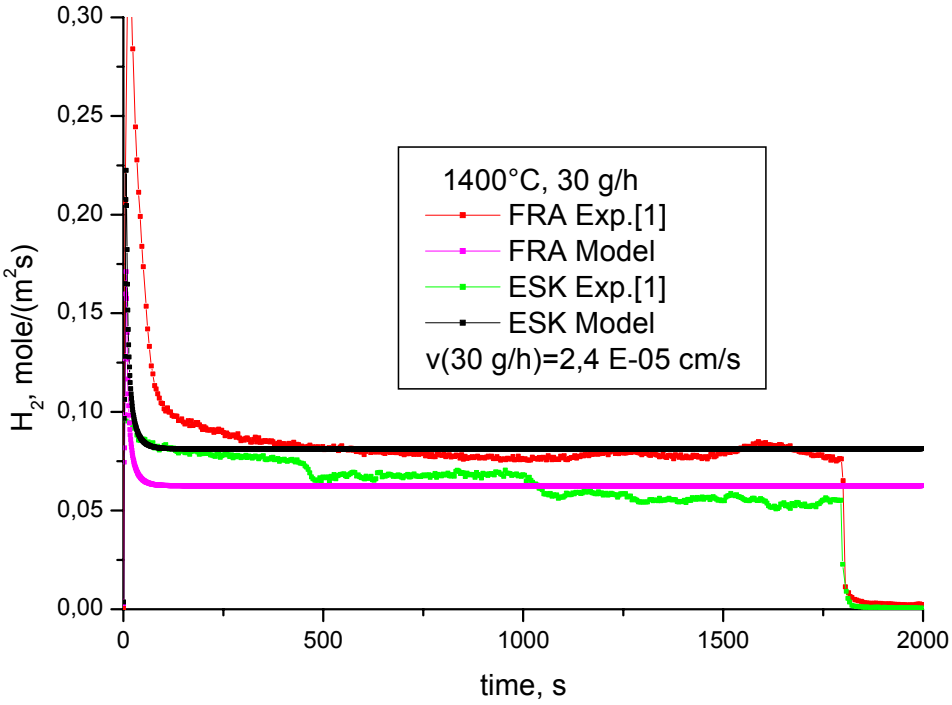

Fig. 20: Experimental results of FRA and ESK samples with the respective simulation model calculation at 1400°C, steam 30 g/h.

7.5 The erosion speed of interface l_1 as a function of Temperature, v(T)

The most perfect samples test to check the code and to calculate the v value as a function of temperature are the ESK samples test, because they have the high density, the lower porosity and the surface exposed is nearer to the sample geometrical surface. The only problem is that the mayor quantities of experimental results are obtained with the FRA samples, particularly those performed at constant temperatures and variable steam partial pressure.

We run the code with the parameters previously defined and v as input value and we obtain the best approach of the experimental results. In Fig.21 the case of ESK sample in steam at 30 g/h=0.4273 bar for Ar 50 l/h and temperature 1000°C is plotted as an example. The hydrogen generated as a function of time during the ESK test was not as constant as we expect. In order to be sure that our calculation always maximizes the hydrogen generated by the reaction, the determination of v value should be either in coincidence with the experimental results or above them.

It is important to note that in ESK sample and for the calculation we use C_{sup}=1 because C_{sup0}=1 and F_{sup}=0, then no correction at all. The initial sharp peak is due to the transient between t=0s, ($\Delta\xi$=0) and the stationary state ~120s ($\Delta\xi$ = cte).

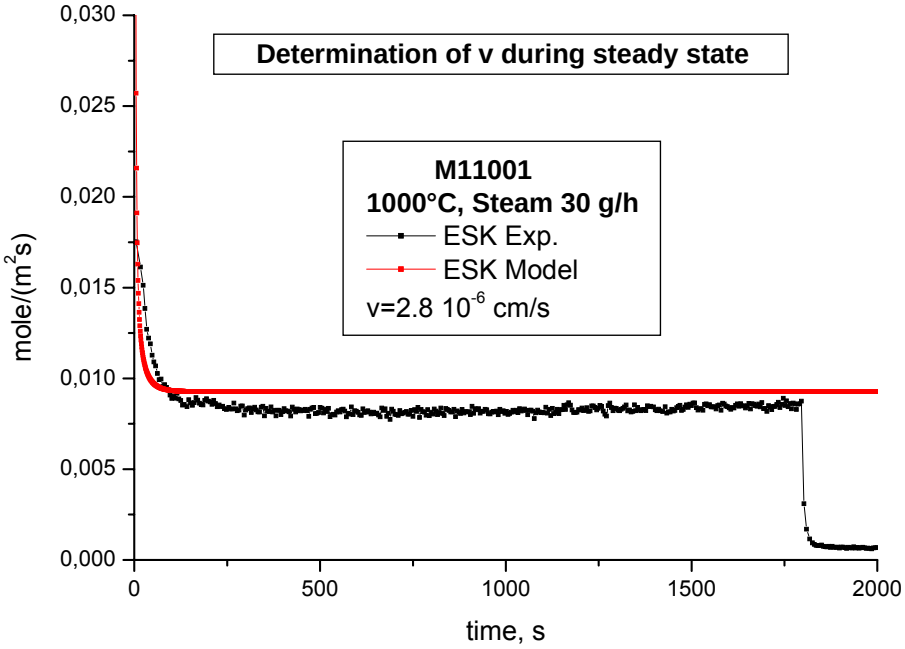

Fig. 21: Determination example of erosion speed, v, of external surface of B_2O_3 (l) during steady state formed over ESK sample. In the case of temperature: 1000°C, steam: 30 g/h, Ar carrier 50 l/h. The M number corresponds to BOX rig experimental denomination [1].

The results are shown in Table 1.

Table 1: Determination of v for different temperatures on ESK samples on steam at 30 g/h, Ar 50 l/h.	
Temperature, °C	v, cm/s
800	$1.5\ 10^{-6}$
1000	$2.8\ 10^{-6}$
1200	$7.0\ 10^{-6}$
1400	$2.4\ 10^{-5}$

The values in Table 1 are plotted in Fig. 22. The results of this plot show us that the reaction we study could be composed of several processes for this plot is not a straight line. Possibly the most simple hypothesis is to think that there are two processes, but this is very difficult to prove with the existing experimental results. Therefore we will try to do our best to describe the four experimental points. We propose an exponential parabolic for the high temperature and an exponential linear function for low temperature:

$$v(T,p=0.4273)=e^{12.67799-59983.29601/T+3.50938E+07/(T*T)} \quad \text{for} \quad 1000°C \leq T \leq 1400°C \qquad (17)$$

$$v(T,p=0.4273)=e^{-9.4373-4262.75236/T} \quad \text{for} \quad 800°C \leq T \leq 1000°C \qquad (18)$$

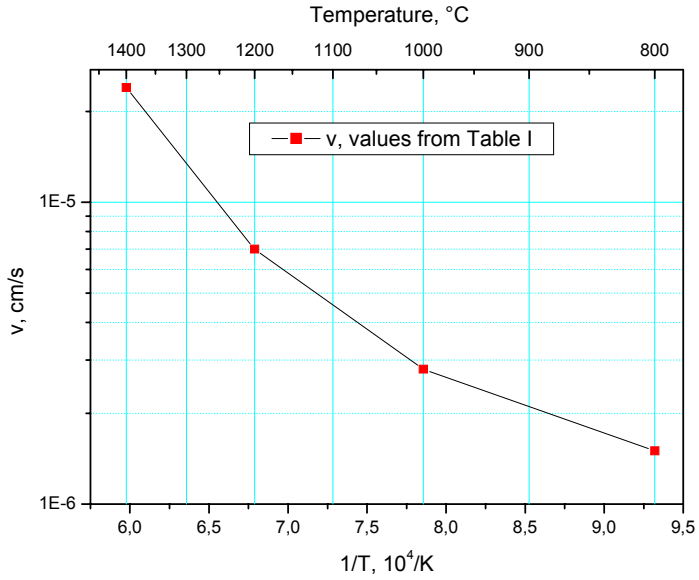

Fig. 22: Log (v) vs. 1/T, steam partial pressure: 0.4273 bar

The exaggerate number of digit in the parameters is only to have the possibility to reproduce the same result, particularly in the points coincident with the experimental temperatures. In the case of transients we consider eq. (18) valid also for temperatures lower than 800°C. For error less than 1%, eq. (17) and (18) becomes:

$$v(T,p=0.427)=e^{12.7-6.E+04/T+3.508E+07/(T*T)} \quad \text{for} \quad 1000°C \leq T \leq 1400°C \qquad (17')$$

$$v(T,p=0.427)=e^{-9.43-4.27E+03/T} \quad \text{for} \quad 800°C \leq T \leq 1000°C \qquad (18')$$

7.6 The erosion speed of interface I_1 as a function of Temperature and Pressure, v(T,p)

We have one experimental result that permits to know the behaviour of the reaction as a consequence of change of steam pressure due to the variation of steam flow rate and constant Ar flow rate, the M10115.

We run the code in order to know the better v, value for each partial steam pressure: 30, 5, 10, 30, 50, and 70 g/h of steam injected in the system with an Ar flux of 50 l/h. The results could be represented by a straight line that passes very near zero for p=0 as a function of steam pressure. Then we consider as a good approximation the eq. (17) and (18) that defines v=v(T) for a partial pressure p=0.4273 bar. We introduce the linear correction for v(T) for steam partial pressure that must be, v(T)=0 when p=0 bar as:

$$v=v(T).p/p_{0.4273} \quad \text{for } T \leq 1400°C \qquad (19)$$

7.7 The meaning of v=0

It is important to note that when, v=0, because p=0, we are dealing with an oxidation process without erosion at the interface I_1, then, an oxidation in air or in Ar+O_2. The system we propose in Fig. 12 is a typical schema that represents the oxygen profile during an oxidation in an oxidant atmosphere able to keep the concentration C_1 constant during all the time. When v=0 the schema valid in our case is just of Fig. 12. In the BOX rig experiment this type of test in oxygen atmosphere was not been performed, this condition will be only useful for some TG test in Ar+O_2. The model proposed will simulate both types of test and also the interaction between steam and Boron Carbide for steam pressure $0>p_{steam}<0.635$ bar. When $p_{steam}=0$ bar the model will simulate the interaction with air (air ingress). In both cases if we need to switch during a kinetics in steam or air to an inert atmosphere we must put $C_1=C_2$ and $p_{steam}=0$ and the system will freeze.

7.8 The oxide layer thickness during steady state as a function of temperature and pressure

We are now able to apply the equation (14) to calculate the oxide layer thickness during steady state for different values of temperature and pressure.

$$\Delta\xi_{t=\infty} = \frac{D}{v}.\ln\left(\left(C_1/C_2\right)\right)$$

Where D=D(T), v = v(T,p) and C_1 and C_2 constant in this case. Then in Fig. 23 we show $\Delta\xi_{t=\infty}$ as a function of T and p. With the parameters selected for the diffusion coefficient, particularly the activation energy, the oxide layer thickness has a similar behaviour (small thickness) at the low and high temperatures considered in the experiments. This was one of the purposes because the high peaks due to surface porosity were attributed to a small oxide thickness, Fig. 23.

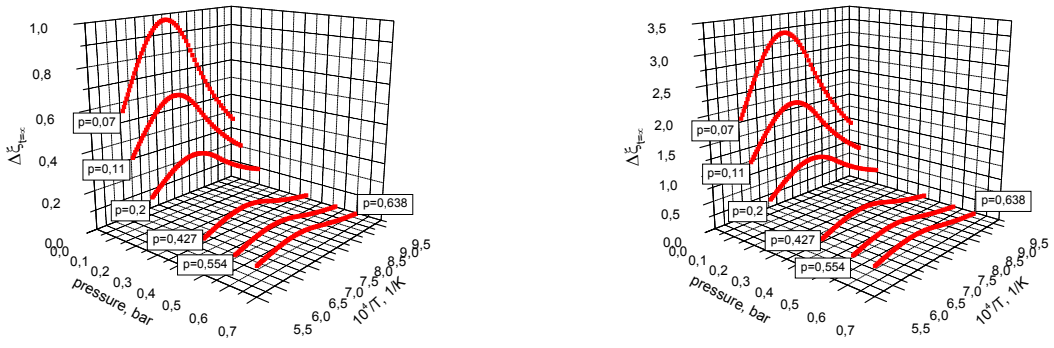

a) b)

Fig. 23: $\Delta\xi_{t=\infty}$ as a function of Temperature and Pressure. a) As a result from the equation (compressed oxide, density 5.9 g/cm^3) b) After expansion, oxide density 1.8 g/cm^3.

7.9 The calculation of hydrogen generated

The hydrogen evaluation generated at any time must be according to the model proposed in §5 for a coordinate system in A:

1) The hydrogen generated at the interface I_1 due to the dissociation of H_2O must provide the necessary oxygen to oxidize the B_4C at the interface I_2 in to B_2O_3:

$$H_2(B_2O_3) = -D_0 \left.\frac{\partial C}{\partial t}\right|_{I_1} \frac{1}{M} \tag{20}$$

2) The hydrogen generated due to C oxidation to form CO_2 at the I_1 interface:

$$H_2(CO_2) = \frac{d\xi_{I_1}}{dt}.2.\frac{\rho_{B_4C}}{M_{B_4C}}. \quad 0.85 \tag{21}$$

3) The hydrogen generated due to C oxidation to form CO at the I_2 interface:

$$H_2(CO) = \frac{d\xi_{I_2}}{dt}.\frac{\rho_{B_4C}}{M_{B_4C}}.0.14 \tag{22}$$

This contribution to the hydrogen generation was already considered in the §7.1 when we calculate the necessary oxygen to oxidize the B_4C and the oxidation of CO in the C_2 value. Then this contribution is included in eq. (20). The values 0.85, 0.14 and 0.01 are average values taken from the experimental results. For the moment the temperature dependence is neglected because it is too small to be considered.

4) The hydrogen necessary to hydrate the C to CH_4 in I_2:

$$H_2(CH_4) = \frac{d\xi_{I_2}}{dt}.2.\frac{\rho_{B_4C}}{M_{B_4C}}.0.01 \tag{23}$$

Then, the total hydrogen generated:

$$H_2(\text{total}) = H_2(B_2O_3) + H_2(CO_2) - H_2(CH_4) \tag{24}$$

Depending on the hypothesis about the surface porosity these values could be multiplied by a C_{sup} factor already defined in §7.4, or by other factor according to the interface considered.

7.10 The calculation of CO_2, CO and CH_4

According to the model proposed in §5:

$$CO_2 = \frac{d\xi_{I_1}}{dt} \cdot \frac{\rho_{B_4C}}{M_{B_4C}} .0.85 \quad (25)$$

$$CO = \frac{d\xi_{I_2}}{dt} \cdot \frac{\rho_{B_4C}}{M_{B_4C}} .0.14 \quad (26)$$

$$CH_4 = \frac{d\xi_{I_2}}{dt} \cdot \frac{\rho_{B_4C}}{M_{B_4C}} .0.01 \quad (27)$$

Depending on the hypothesis about the surface porosity these values could be multiplied by a factor C_{sup}, already defined in §7.4, or by other factor according to the interface considered.

7.11 Weight calculation of the sample

The total weight of the sample as a function of time in system A, Fig. 13 is:

If v=0: $W_{v=0} = \xi_{I_2} . \rho_{B_2O_3} - \xi_{I_2} . \rho_{B_4C}$ (28)

If v>0: $W_{v>0} = (\xi_{I_2} - \xi_{I_1}) . \rho_{B_2O_3} - \xi_{I_2} . \rho_{B_4C}$ (29)

To obtain the results in mg/cm^2, 10^3 must multiply both equations, because the interface positions are in cm and the densities in g/cm^3.

8. Principal characteristics of the model proposed

The model we propose must be able to simulate BOX rig experiments as well as TG ones. This paragraph is dedicated to show the influence of different model variables on the kinetics results.

8.1 Results type BOX rig

The different results in the BOX rig test show peaks at the beginning of the reaction with different characteristics, as we discussed previously §7.4. The purpose is now to show the influence of oxygen diffusion coefficient in this initial peak.

8.1.1 Isothermal test

The initial peak is due to the acceleration of interface I_2 to reach the equilibrium position at any time. It is well known that during the parabolic kinetics, v=0, also the I_2 interface has an infinite speed at t=0.

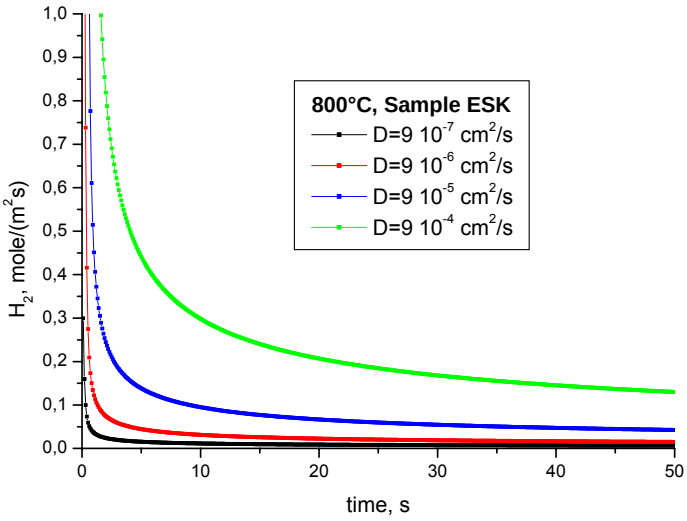

Fig. 24: Shows the influence of different oxygen diffusion coefficients in the sharp initial H_2 peak.

This is the same case but the speed must be bigger because the interface I_1 has already the speed v (if we consider the system from coordinates fixed to A, §5.1, Fig. 25 or Fig. 27c. On the contrary, from coordinates fix to B, the speed will be lower than the parabolic one, Fig. 27b. The influence of different D_O values is shown in Fig. 25. The $D_O(800°C)=3.5\ 10^{-8}$ cm^2/s is a lower value than those used in Fig. 25. Nevertheless a factor 10^3 is not able to produce an initial peak comparable with those showed in §7.4. It only grows up to 10 s (at 0.3 mole/(m^{2}s)) for a factor bigger than of 10^3 in D_O.

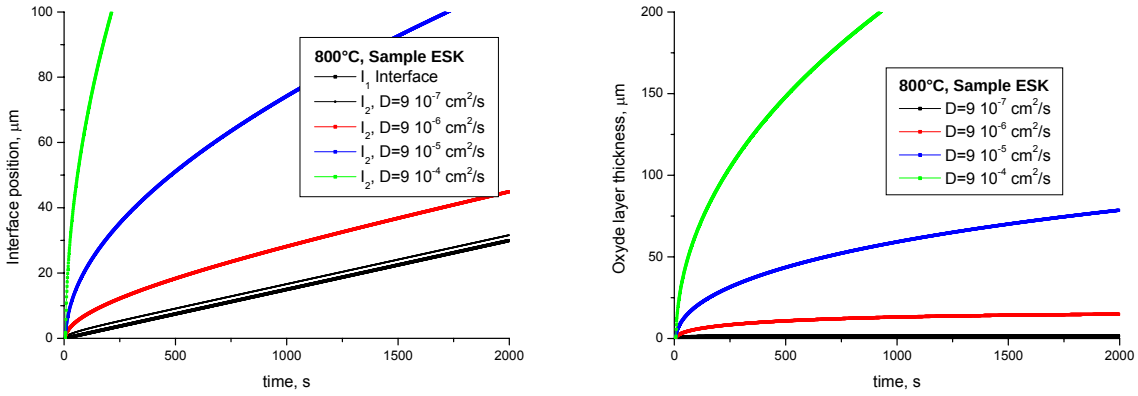

b) c)

Fig. 25: Shows the influence of different oxygen diffusion coefficients in the oxide. a) in the interface positions (System reference A), b) in the oxide layer thickness.

It is also important to observe in Fig. 25b, that during steady state I_2 travels at the same speed than I_1, both at speed v, independent of the value of D_O. Then, in BOX rig isothermal test, D_O has no influence on the H_2 generation during steady state.

The value of the parameter v determines the H_2 production during steady state in BOX rig isothermal test.

8.1.2 The different non condensable molecules intensities according to the model proposed

If we consider all the non condensable gases according to the distribution previously mentioned in §7.9, the H_2, CO and CH_4 present the typical peak in surface but the CO_2 is constant, related to the interface at which this species is generated.

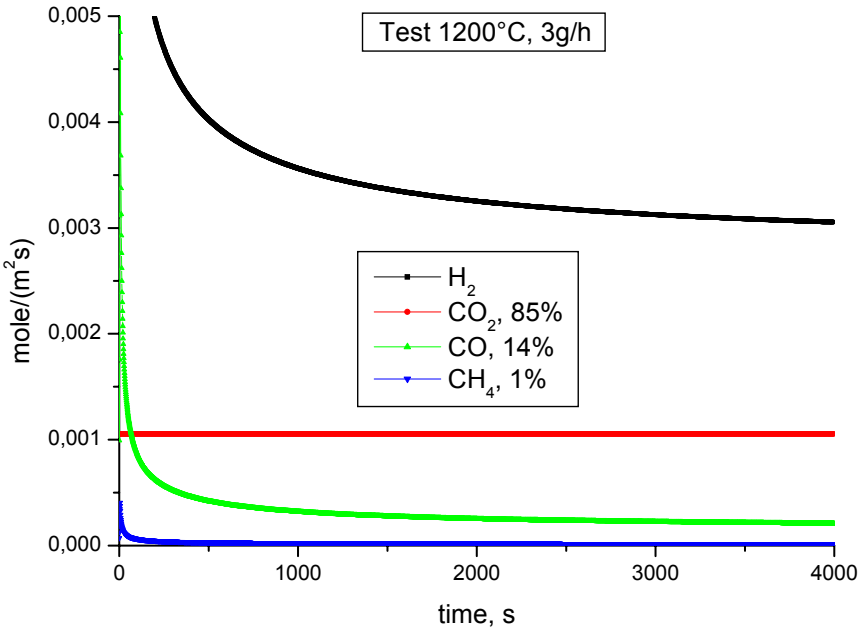

Fig. 26: Kinetics behaviour of each non-condensable gas as a function of time.

This behaviour Fig. 26, shows a difference related with the origin of the gaseous products. It does not simulate the comportment of the species of §4.1. It seams that the efficiency of CO_2 formation depends on the Carbon concentration in the boron oxide. The erosion speed v of interface I_1 does not seem to be accompanied by formation of CO_2 according to the Carbon that is dissolved in the oxide. Then when the kinetics starts, the quantity of CO_2 is very low and the Carbon begins to be accumulated in the oxide. The efficiency to generate CO_2 increases due to this accumulation. Therefore and as a function of time the Carbon in the oxide will reach an equilibrium concentration and the CO_2 generation will become constant.

8.1.3 Results type TG

In the case of TG results, the D_O and v have an important influence on the oxide layer thickness and then in its kinetics. In Fig. 27 we show different TG simulations for a given D_O and different v. For v=0 we have a parabolic gain of weight, typical oxidation in air or Ar+O_2 and also a parabolic oxide layer thickness growth. If we change D_O we will have different parabolic behaviours. When v>0 the parabolic behaviour is lost and from t=0 up to steady state we have a transient approaching later a straight line where its slop reaches the speed v. From that moment the oxide layer thickness is constant, Fig. 27b.

Fig. 27c, shows the different speed at the beginning of the kinetics between similar samples and conditions except the atmosphere in Ar+O_2 (air) v=0 and Ar+Steam v=5.10^{-6} cm/s>0. The sample into steam atmosphere, v>0, has always more interface speed then it generates a sharper hydrogen peak (dl_2/dt) than a parabolic kinetics one, v=0. The bigger is the v value, sharper and higher is the hydrogen peak.

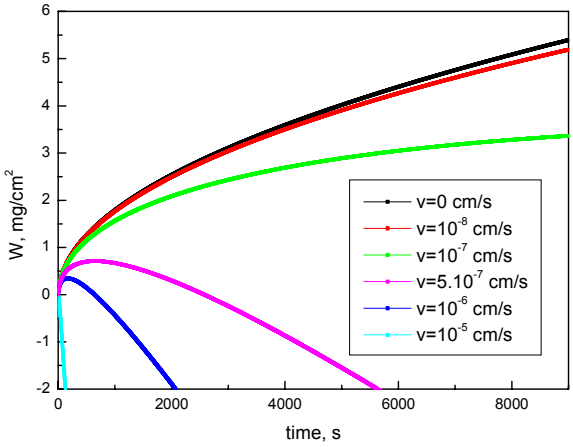

a)

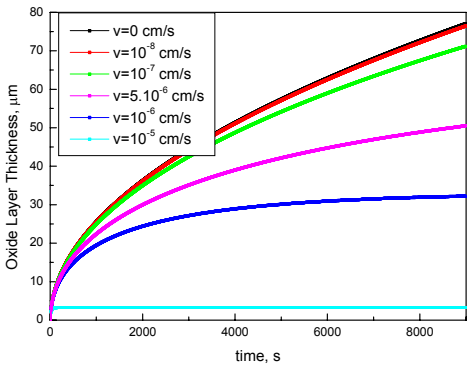

b)

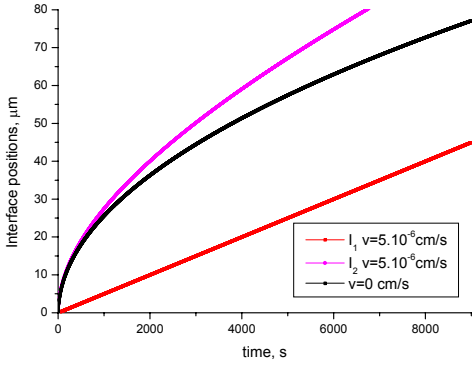

c)

Fig. 27:: Simulation of possible TG results of ESK sample for different values of v and constant temperature. a) Weight vs. time b) The corresponding oxide layer thickness vs. time. c) Interface positions in the case of v=0cm/s and v=5. 10^{-6}cm/s. System reference A.

Fig. 28 shows the influence of v in the case of FRA sample. In this case we introduce the factor C_{supI} like in eq (28) and (29) in the place of C_{sup} defined:

$$C_{supI} = \int_0^t C_{sup}\,dt \qquad (30)$$

The results are very similar to those obtained in the case of ESK samples (no porosity) but with extra weight at the beginning of the kinetics due to the accumulation of B_2O_3 liquid in the superficial sample porosity like we show schematically in Fig. 18. The eq. (30) shows that the extra oxide generated by the big surface porosity is kept in the sample during the kinetics.

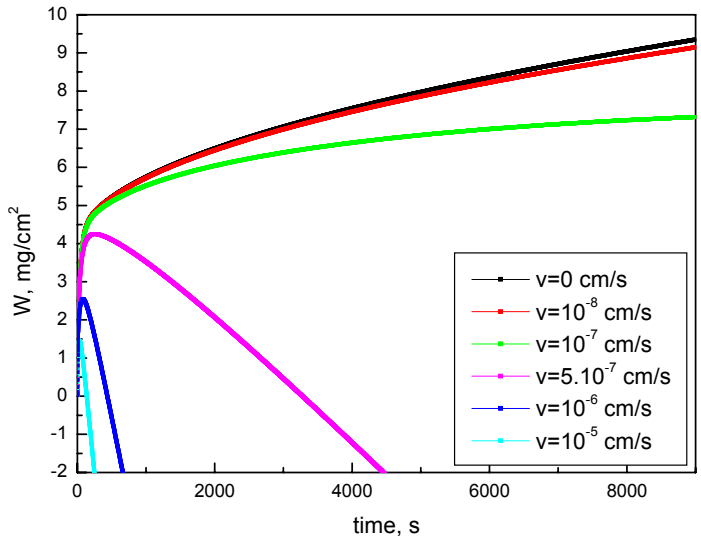

Fig. 28: Simulation of possible TG results of FRA sample for different values of v and constant temperature. Oxidation in air ($Ar+O_2$), v=0.

9. Model Results

With the previously defined v(T,p), the roughness surface enhanced by the porosity S_{sup} and C_{sup0}, the oxygen diffusion coefficient in the boron oxide D_O and the oxygen concentration in each interface C_1 and C_2, it is possible to execute the computer code in order to compare the model with the different experimental results.

9.1 The isothermal BOX rig test

9.1.1 The FRA samples

The FRA samples we simulated are: steam 30 g/h with the adequate C_{sup} defined by Sup. Fact., t_0 and σ and C_{sup0}. Fig. 29 shows these simulations in comparison with the experimental test.

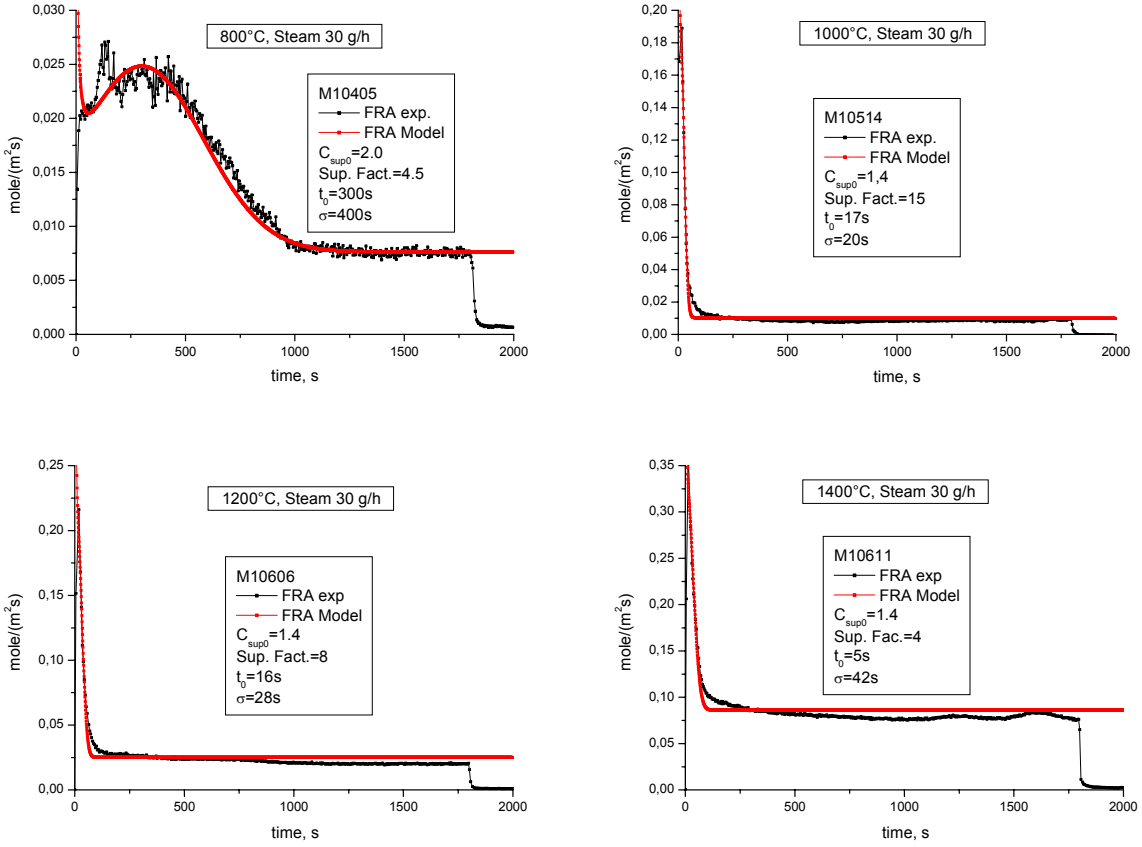

Fig. 29: Experimental and model results of FRA samples at different temperatures, constant steam flux of 30 g/h and 50 l/h of Ar carrier. The M number corresponds to BOX rig experimental denomination [1].

We performed a similar treatment for FRA samples and steam of 3 g/h. Fig. 30 shows these simulations in comparison with the experimental test.

The results are acceptable particularly in the case of 3 g/h because the v values are the result of interpolation by a straight line between v(T, p=0.427 bar) and v(T, p=0 bar).

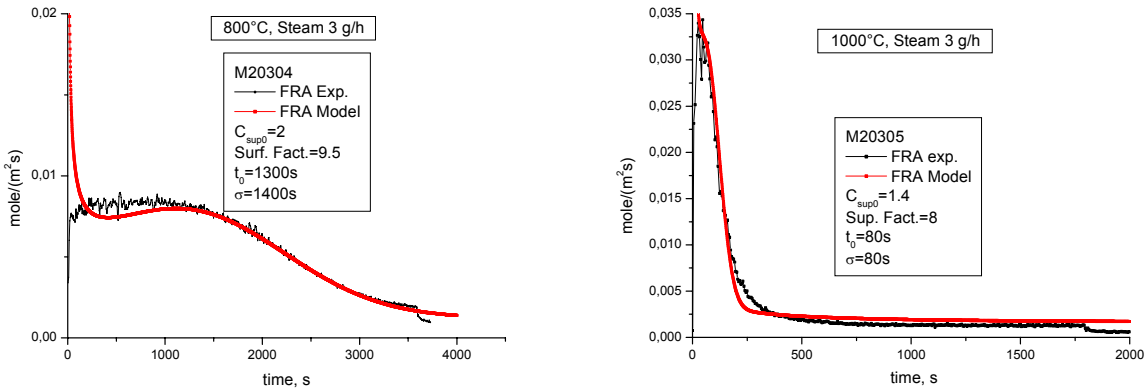

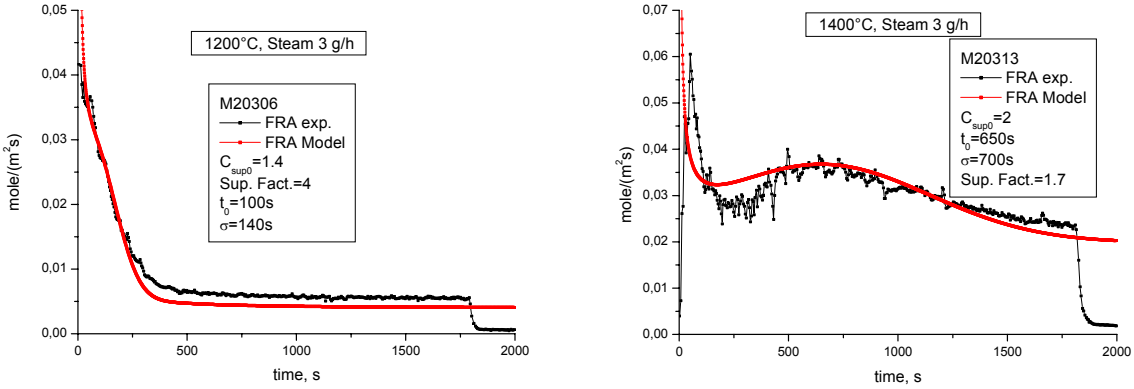

Fig. 30:: Experimental and model results of FRA samples at different temperatures, constant steam flux of 3 g/h and 50 l/h of Ar carrier. The M number corresponds to BOX rig experimental denomination [1].

9.1.1.1 The initial peak in the FRA samples

To evaluate the importance of initial peak in the FRA samples over the total hydrogen produced, we integrate the C_{sup} and we plot it as a function of temperature, Fig. 31. As we show previously the major influence is produced at low temperature, 800°C and at high temperature 1400°C especially for 3 g/h of steam. In the case of steam 30 g/h the behaviour is more constant as a function of temperature.

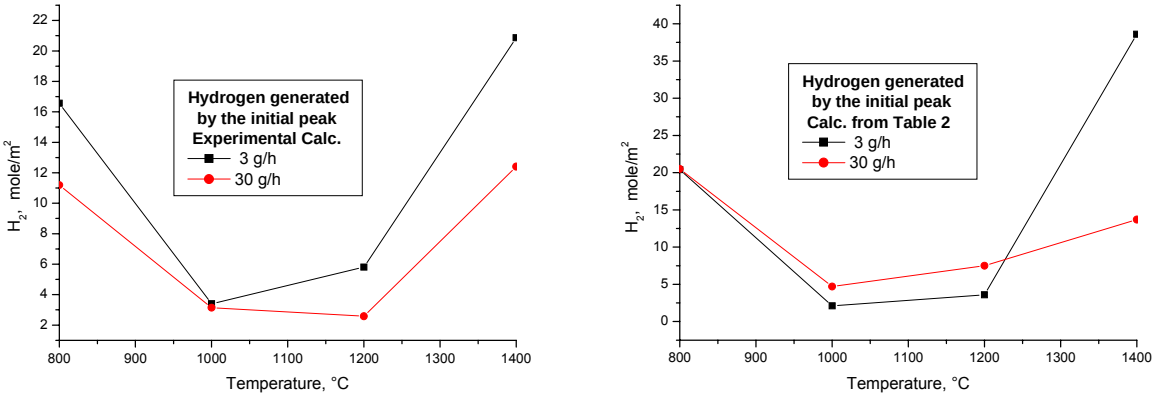

a) b)

Fig. 31: Hydrogen generated by the initial peak of FRA samples for 3 and 30 g/h of steam. a) Calculation from experimental data. b) Calculation from Table 2 data.

We are now able to evaluate for each temperature the time necessary to produce an equivalent quantity of hydrogen during steady state. This time measures the importance of initial peak in comparison with the hydrogen generated later at the same temperature during steady state in FRA samples, Fig. 32.

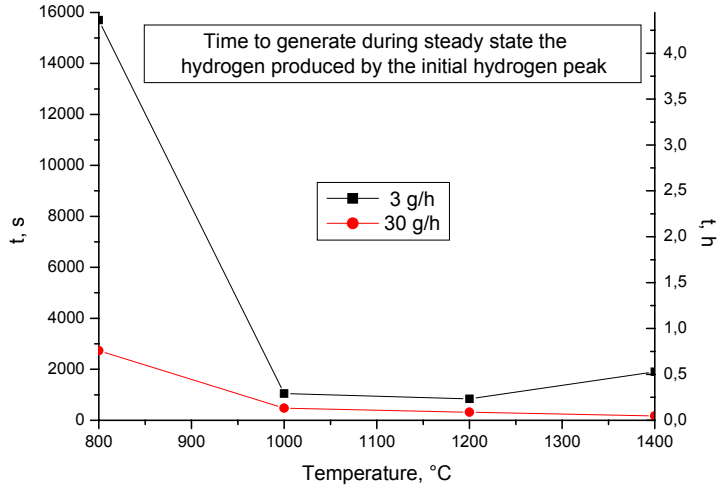

Fig. 32: The time necessary to generate, during the steady state, the equivalent quantity of hydrogen produced during the initial peak in FRA samples at constant temperature, for 3 and 30 g/h of steam.

The most important initial peak is produced at 800°C. 4.4h will be necessary during steady state at 800°C to generate a similar quantity of hydrogen. In this case it seems impossible to neglect the initial peak while calculating the hydrogen generated at 800°C, except for very long time experiment >4.4.h.

9.1.1.2 The parameters that define the initial peak in FRA samples

In Table 2 we will find the parameters used to simulate the initial peak in FRA samples.

Table 2: Parameters used in §9.1.1 necessary to reproduce the initial peak in FRA samples

	800°C	1000°C	1200°C	1400°C	
3 g/h	9.5	8	4	1.7	Sup. Fact.
	1300	80	100	650	t_0, s
	1400	80	140	700	σ, s
	2.0	1.4	1.4	2.0	C_{sup0}
30 g/h	4.5	15	8	4	Sup. Fact.
	300	17	16	5	t_0, s
	400	20	28	42	σ, s
	2.0	1.4	1.4	1.4	C_{sup0}

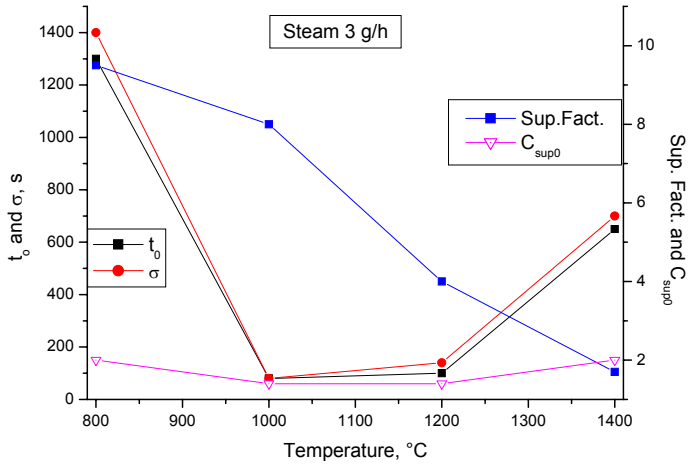

Fig.33: Parameters of Table 2 for steam 3 g/h as a function of temperature.

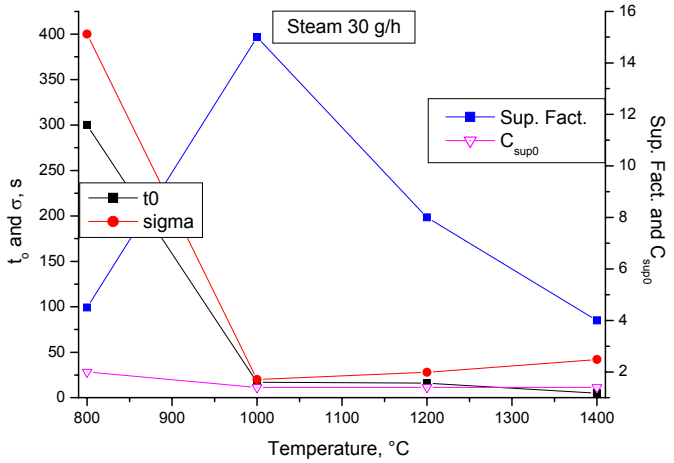

Fig. 34: Parameters of Table 2 for steam 30 g/h as a function of temperature.

In Fig. 33 and Fig. 34, we represent the parameters of Table 2 as a function of temperature.

The behaviour of t_0 and σ are similar as a function of temperature, with high values for 800°C and 1400°C in the case of steam 3 g/h and also high values for 800°C for steam 30g/h.The comportment of Sup. Fact. (3g/h) is strongly dependent of temperature, very high for 800°C and low for 1400°C. In the case of 30 g/h it has the same growth tendency from high temperature, 1400°C, up to 1000°C but it decreases for 800°C. The values of C_{sup0} vary only between 1.4 and 2.0 and they are related with porosity therefore with the surface increased at I_2 interface

The parameters t_0 and σ are related with the permanence time of initial peak on FRA kinetics. We suppose that the oxide layer thickness during steady state, ξ_{inf}, is associated with these parameters. In Fig.35 we show the behaviour as a function of temperature of $1/\xi_{inf}$ from Fig. 23b. It is possible to observe a similar behaviour between $1/\xi_{inf}$ and t_0 and σ. The thinner is the oxide layer the more the time will take the oxide to cover the surface with an approximately surface value near the one of the geometrical surface, Fig. 27 and Fig. 18.

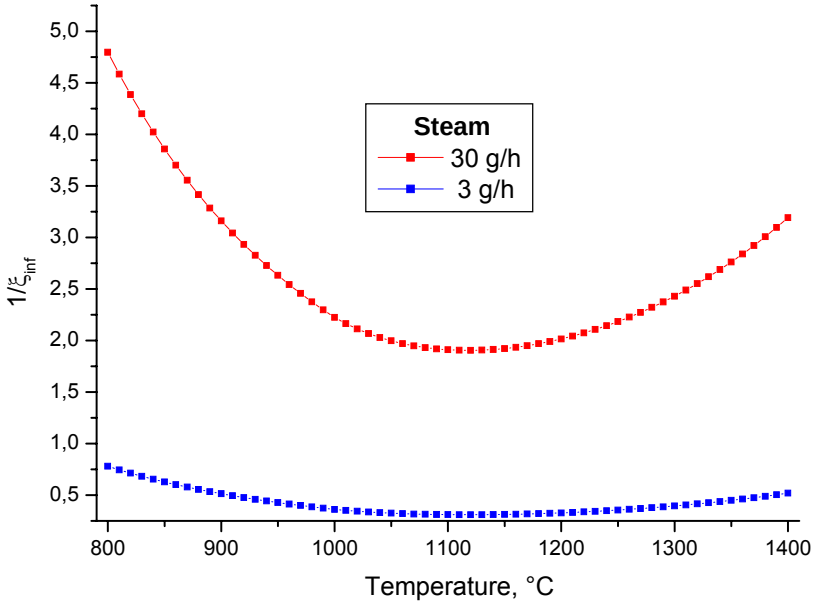

Fig. 35:: $1/\xi_{inf}$ vs. temperature, ξ_{inf} calculated from data of **Fig. 23b**.

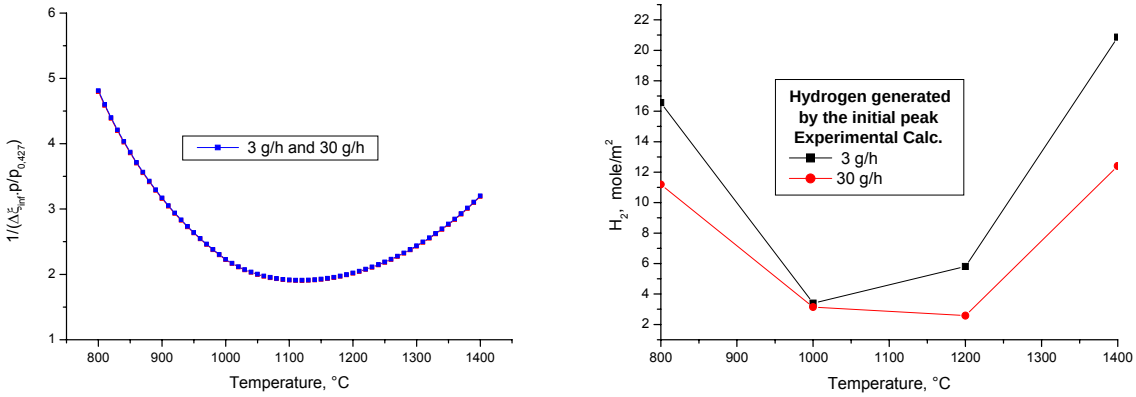

a) b)

Fig. 36: a) Similar calculation Fig. 35 but now $1/(\Delta\xi_{inf}.p/p_{0.427})$ vs. Temperature. b) The hydrogen generated by the initial peak.

It is clear from these results that it does not exist a good correspondence in intensity of t_0 and σ between 3 and 30 g/h. In Fig. 33 the values for 3 g/h are bigger than the values in Fig. 34 for 30 g/h. On the contrary in Fig. 35 the values for 30 g/h are bigger than the 3 g/h. **Fig. 36** shows another approach corresponding better to the behaviour of Fig. 36b but more difficult to interpret without a model. Nevertheless, the initial peak on FRA samples seems to be related with small boron oxide layer thickness.

9.1.2 The ESK samples

The ESK samples we simulate are: steam 30 g/h with C_{sup}=1, because Sup. Fact. = 0 and C_{sup0}=1. Fig. 37 show these simulations in comparison with the experimental test.

A similar treatment we perform for ESK samples and steam of 3 g/h. Fig. 38 show these simulations in comparison with the experimental test.

The results are also acceptable because the v values are the consequence of interpolation by a straight line.

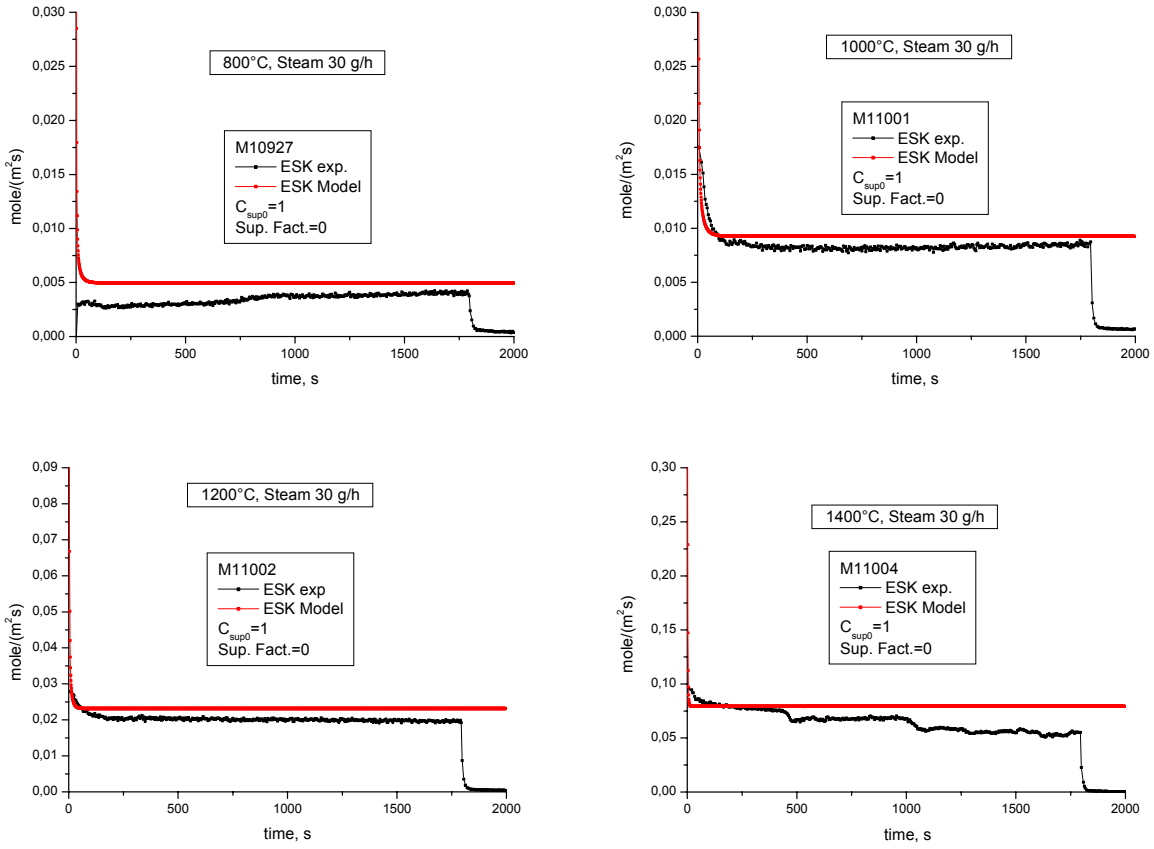

Fig. 37: Experimental and model results of ESK samples at different temperatures, constant steam flux of 30 g/h and 50 l/h of Ar carrier. The M number corresponds to BOX rig experimental denomination [1].

9.1.3 The pressure transients

The steam pressure transients were performed at 1200°C and the hypothesis of steam pressure linearity in bar is confirmed. This is the only case in the BOX rig tests where the influence of the oxygen diffusion coefficient value is important. In the kinetics case, Fig.39a, a factor two in the diffusion coefficient changes the approach to the steady state value, if we increase this value the steady state will be not reached during each period of 300s where the system is keeping at constant steam pressure. In Fig.39b as we show previously in §5.1, eq.

14, the value of the oxide layer thickness will increase the same factor than the diffusion coefficient. This also shows that the time to reach the steady state will increase too.

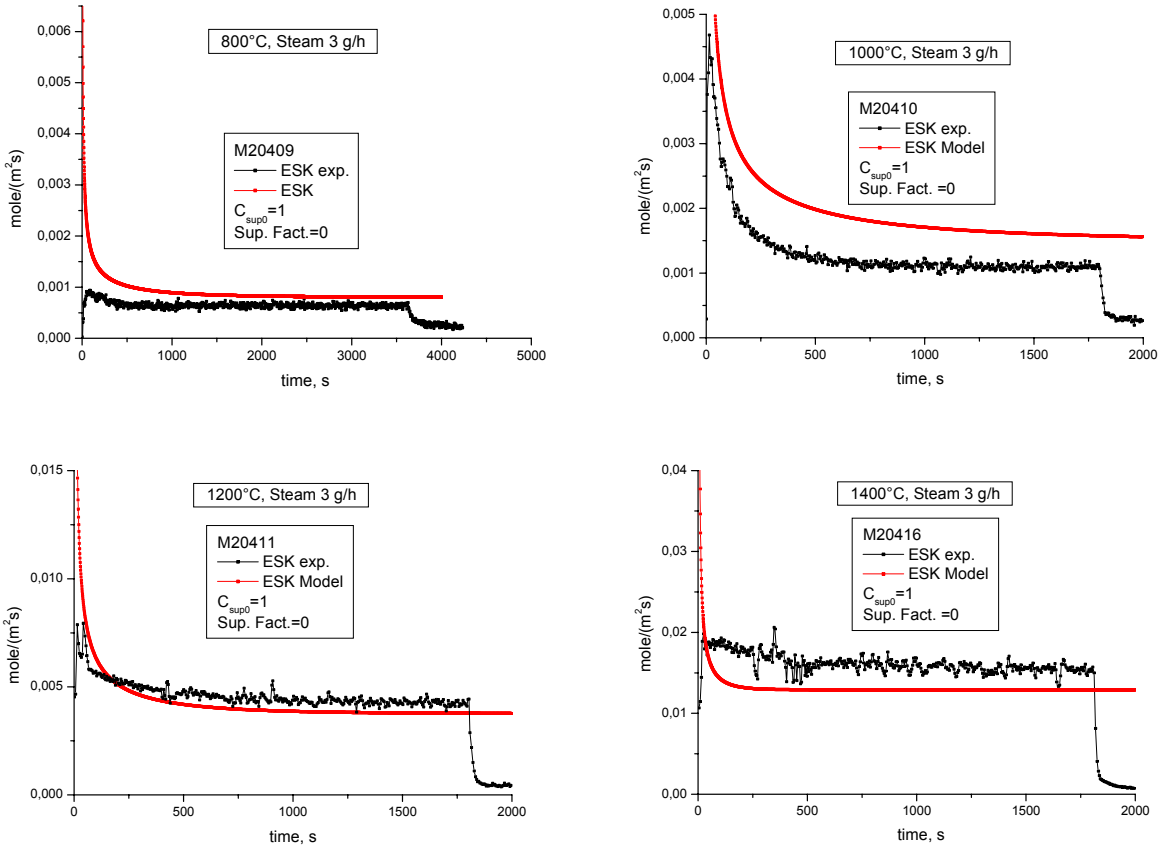

Fig. 38: Experimental and model results of ESK samples at different temperatures, constant steam flux of 3 g/h and 50 l/h of Ar carrier. The M number corresponds to BOX rig experimental denomination [1].

Therefore, if we increase too much the diffusion coefficient the step function obtained during the test will not be achieved. We will later show in the case of TG test, §9.3, which if the diffusion coefficient is too low the TG tests are not simulated. Then we have lower and upper values for the diffusion coefficient.

For these FRA samples no correction was necessary, perhaps because, like in the constant pressure tests, the steady state is not achieved. In this case we do not use any superficial correction neither for the initial peak nor for the permanent FRA samples in interface I_2: the factor C_{sup0}=1. Nevertheless the fit is acceptable. The reason is showed in Fig. 40, the differences between two experimental results at similar conditions for the period (0s-600s) are not in coincidence. This could be attributed to a different surface porosity or different degree of surface contamination. In the case of Fig. 39, compensate the factor, C_{sup0}, defined previously.

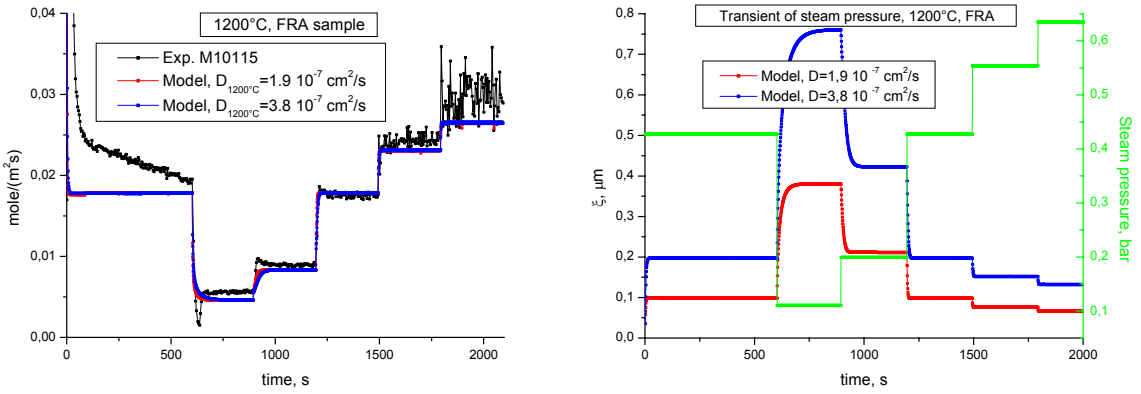

a) b)

Fig. 39: a) Experimental and model results of FRA samples at different temperatures, variable steam flux of 30, 10, 30, 50 and 70 g/h and 50 l/h of Ar carrier. Two diffusion coefficients were used to show its influence. The M number corresponds to BOX rig experimental denomination [1].
b) Showing the influence of diffusion coefficients on the oxide layer size. The value of $D_O(1200°C)=3.8\ 10^{-7}$ cm^2/s corresponds to definition in §7.3.

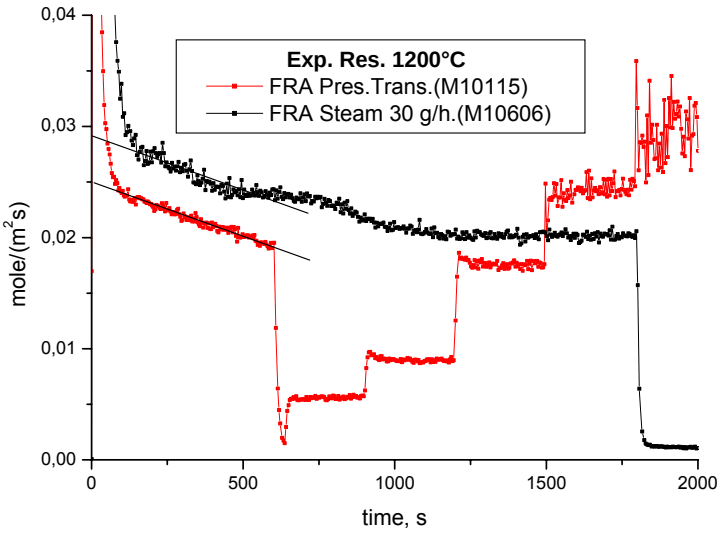

Fig. 40: The FRA samples from 0s to 600s are under similar conditions of pressure and temperature. The difference corresponds at a factor 1.23 at t=600s. The M number corresponds to BOX rig experimental denomination [1].

9.2 The transients temperature BOX rig test

Different transient temperature tests were performed in the BOX rig. The sample support that was later modified §0 was the most used. The only transient performed with the new support

was M10406, which during a cool-down phase suffered an off-gas pipe blocked. In Fig. 41, we simulate this transient with the model proposed.

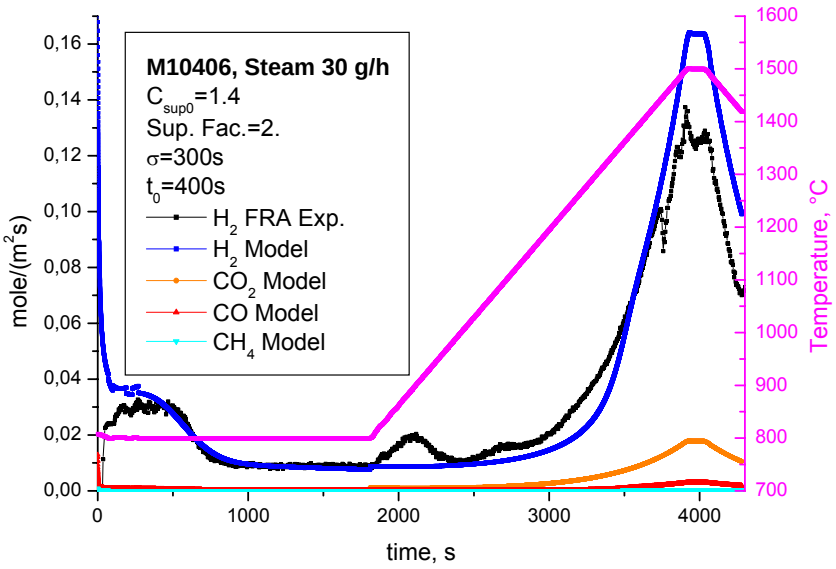

Fig. 41: The transient temperature test with a constant period (0s-1820s) at 800°C and heat up at 1500°C in 2100s, 110s at 1500°C and after cool down at the same speed. The M number corresponds to BOX rig experimental denomination [1].

During a cool-down phase the BOX rig suffers an off-gas pipe blocked at 1420°C.

The model results for CO_2, CO and CH_4 are also plotted. The initial hydrogen peak was simulated as always but the peak at 890°C and 1085°C does not appear in this simple model. This could be attributed to a change in the physical properties in the liquid oxide like density or viscosity that could influence the way to cover the irregular FRA samples surface, then the erosion speed of the external surface. It is important to notice that the sharp peak between 0s and 100s generates 8.3 mole/m^2. If we consider that the surface peak has a value of 0.036 mole/(m^2s), which is 3.6 mole/m^2 of hydrogen, the sharp peak contributes with 4.7 mole/m^2. This peak is not considered in the calculations of Fig. 31b and does not appear in the experimental results perhaps because it is very sharp (for 30 l/h of steam). The detection with the mass spectroscopy is obtained through a length tube of 2.7m with an inner diameter of 6mm.

9.3 The isothermal thermogravimetric test

A series of thermogravimetric (TG) tests was performed [2] to elucidate the different mechanisms presented in the interaction between B_4C with oxygen and steam, always using Ar as a carrier gas. In this case the way to introduce the gas mixture was different than in the BOX rig. A pure Argon supply was divided in two streams: first, a standard gas flow of 10 l/min Ar through the balance housing was introduced in the thermobalance to prevent the sensitive unit from the highly corrosive reaction products and humidity, and secondly a

reaction gas bubbling in a water bath at given temperature inlet near the reaction zone was added. We will now intend to simulate the TG test in Ar + Steam atmosphere with the same parameters determinate with the BOX rig experiments.

9.3.1 The oxidation in Argon + Steam atmosphere

The TG analysis, Fig.42, shows the mass evolution of a dense (ESK) B_4C pellet during oxidation in Ar-Steam with flow rate 20 l/h and a partial pressure of about 100mbar H_2O. The authors mention, "…for long test duration, formation of a new B_2O_3 is constant and equal to the evaporation of B_2O_3. The reaction is governed by diffusion controlled oxidation with parabolic kinetics and linear kinetics in evaporation". We use the same model as before with the same constant determined by BOX rig simulation: v(T,p), D_O, densities of boron oxide and boron carbide and C_1 and C_2, $\Delta C = C_1-C_2$. In order to have a good agreement with the experiment it was necessary to reduce the Steam partial pressure to a value of 27.3 mbar instead of 100 mbar mentioned for the authors. For short times the disagreement is important, but the fact that the experimental results show an inflexion point before approaching the slope for longer times, induces us to think that the first part could be produced by a buoyancy effect in the balance during heat up phase.

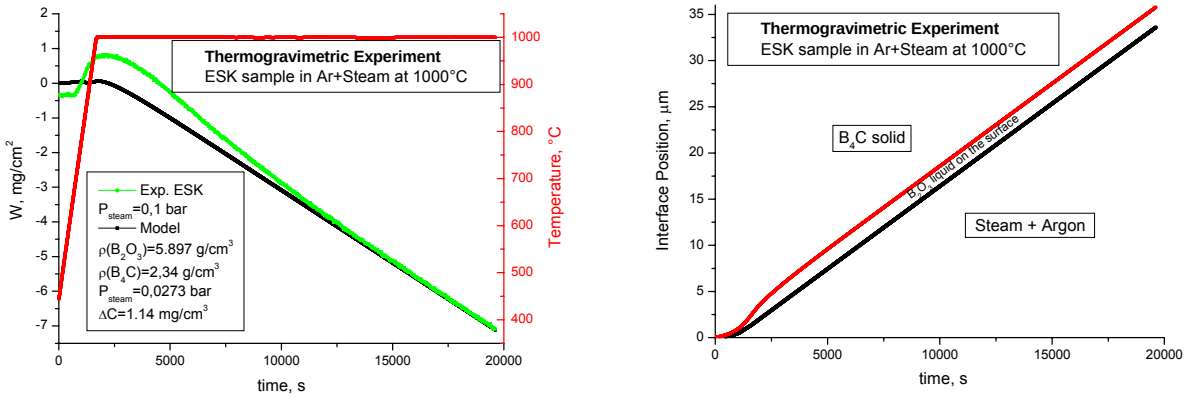

a) b)

Fig. 42: Model approach of the TG test at 1000°C of ESK sample in an Argon + Steam atmosphere. a) Comparison with the experimental result [2] showing the principals data used. b) The corresponding interfaces positions as a function of time.

9.3.2 The oxidation in Argon + Oxygen atmosphere

Fig. 43 shows a typical parabolic oxidation behaviour except for the first seconds where a possible buoyancy effect takes place. The model matches the experimental results but it was necessary to perform a minimum change in the ΔC value. $\Delta C=1.54$ mg/cm^3 instead of $\Delta C=1.14$ mg/cm^3 used up to now. It is the first time we intend to simulate an oxidation where v=0 (no Steam) and perhaps even the boron oxide are not the same in absence of steam with respect to the oxygen diffusion coefficient. This could be the reason of small change in ΔC.

A similar experiment was also performed in Argon + Oxygen atmosphere but in this case at 1300°C. It seems that due to the high temperature the boron oxide changes some of its own characteristics like viscosity and the ability to keep added on the B_4C as a uniform layer. Therefore, only a certain oxide liquid thickness is able to be added to the sample surface.

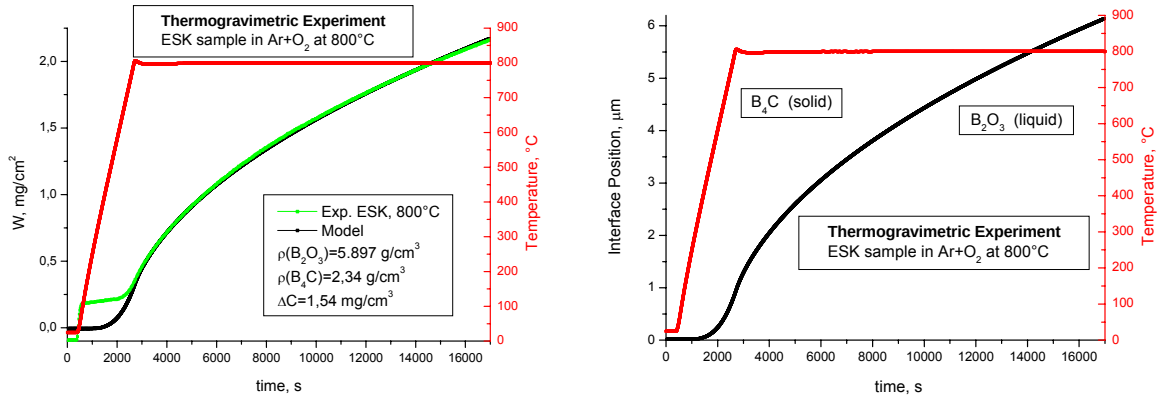

a) b)

Fig. 43: Model approach of the TG test at 800°C of ESK sample in an Argon + Oxygen atmosphere. a) Comparison with the experimental result [2] showing the principals data used. b) The corresponding interfaces positions as a function of time.

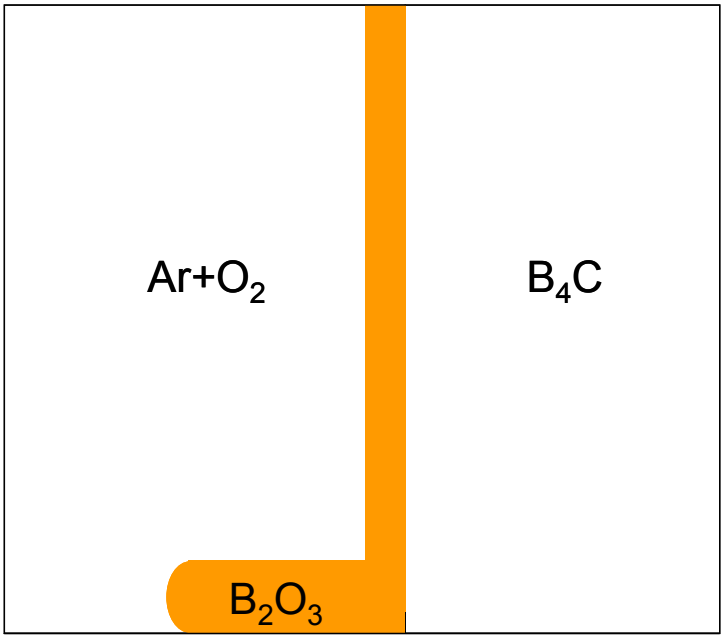

Fig. 44: Schematic representation of maximum liquid oxide layer over the surface of B_4C. The excess of liquid oxide is collected by the support and it must be considered in the total weight of the sample.

The excess of liquid oxide falls off as we show in Fig. 44, the total liquid oxide generated is measured by the balance. We don't have any experimental information about the maximum

liquid oxide layer thickness able to stay on the surface. However this parameter is necessary to adjust the kinetic experimental result, Fig. 45. The model simulates in a satisfactory way the kinetics with a value of v=3.4 10^{-7} cm/s and a ΔC=2.4 mg/cm^3 with an equilibrium liquid oxide layer thickness of about 10 µm in a non-expanded model. If we expand the B_2O_3 at 1.8 g/cm^3 the thickness is about 32.7 µm.

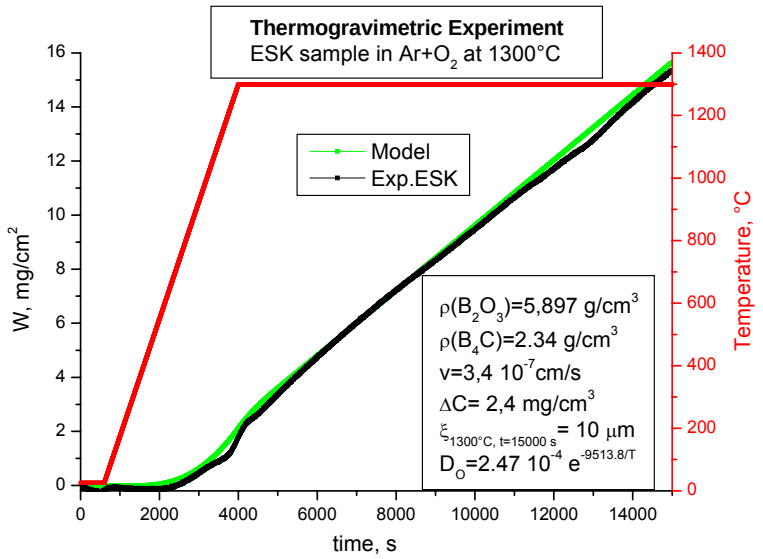

a)

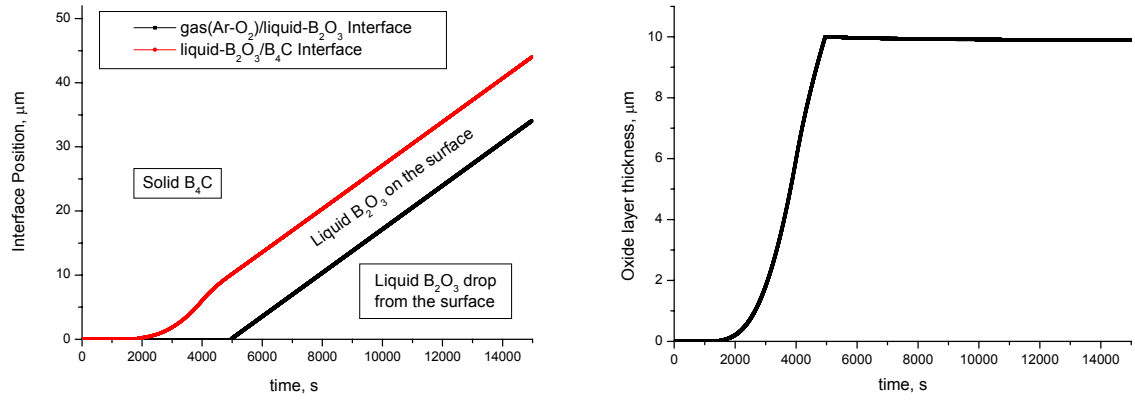

b) c)

Fig. 45: Model approach of the TG test at 1300°C of ESK sample in an Argon + Oxygen atmosphere. a) Comparison with the experimental result [2] showing the principals data used. b) The corresponding interfaces positions as a function of time. c) The oxide layer thickness as a function of time.

In these two last experiments we will have to increase ΔC that in the case of BOX rig simulations was always 1.14 to 1.54 and 2.4 mg/cm^3 respectively. This means to keep the original ΔC=1.14 mg/cm^3 and to increase a little the diffusion coefficient. This leads us to conclude that in the case of oxidation in Ar+O_2 the oxygen diffusion coefficient must be bigger than an oxidation in Ar+Steam but not lower. It gives a lower limit for the diffusion coefficient.

10. Reduced time calculation to simulate the interaction

The previous experimental results and the modelling proposed about the interaction between Boron Carbide with Steam and Air show that the modelling approach of oxygen diffusion through the Boron Oxide formed on the surface of Boron Carbide is able to simulate the BOX rig experimental results and the Thermogravimetric test. It also shows that the calculation time was important to be implemented in accidents codes. In the next paragraph we will propose a simple equation able to reproduce the experimental results in the case of BOX rig experiments and for the generation of non-condensable gases during the interaction between boron carbide and steam.

10.1 Reduced time equation for calculation of H_2, CO, CO_2 and CH_4 generation during steady state

We will give priority to obtain good results in the case of non-condensable gases generation at constant temperature or during temperature transients. Simultaneous steam pressure changes add the initial peaks particularly in the case of hydrogen.

The main equation during steady state from the model proposed for the oxide layer thickness was eq. (14):

$$\Delta\xi_{t=\infty} = \frac{D}{v}.\ln\left(\left(C_1/C_2\right)\right)$$

where D = D(T) and v=v(T).p/p_0, where p_0 is the reference considered p_0=0.427 bar. C_1 and C_2 are the maximum and the minimum oxygen concentration in Boron Oxide.

From eq. (24) we have the total hydrogen necessary to oxidize B_2O_3, CO_2 and CH_4. The hydrogen to oxidize CO was already considered in the term $H_2(B_2O_3)$, see §7.1:

$$H_2(\text{total}) = H_2(B_2O_3) + H_2(CO_2) - H_2(CH_4)$$

Then, we will calculate each term in the case of steady state, eq. (20):

$$H_2(B_2O_3) = -D_O \cdot \left.\frac{\partial C}{\partial x}\right|_{I_1} \cdot \frac{1}{M_O} \approx D(T).\frac{\Delta C}{M_0 \Delta\xi_{t=\infty}}$$

where $\Delta C = C_1 - C_2$. We approximate the derivative for the straight line between C_1 and C_2. This approximation does not introduce any important error because trough the previous results analysis we found in each case almost a straight line.

From eq. (21) and in steady state the speed of interface I_1 is equal to the speed of interface I_2 and equal to v:

$$H_2(CO\ ) = 2.v(T,p).\frac{\rho_{B_4C}}{M_{B_4C}}.0.85$$

From eq. (23):

$$H_2(CH_4) = 2.v(T,p).\frac{\rho_{B_4C}}{M_{B_4C}}.0.01$$

The total hydrogen generated due to the formation of B_2O_3, CO, CO_2 and CH_4 is:

$$H_2(\text{Total}) = v(T,p).(\Delta C/M_O/\ln(C_1/C_2) + 1.68\,.\,\rho_{B_4C}/M_{B_4C}).C_{sup0} \qquad (31)$$

From eq. (17') and (18') we know $v(T,p_0)$

$v(T,p)=v(T,p_0).p/p_0= p/p_0*e12^{-7-6.E+04/T+3.508E+07/(T*T)}$ for 1000°C≤ T≤ 1400°C

$v(T,p)=v(T,p_0).p/p_0= p/p_0*e^{-9.43-4.27E+03/T}$ for 800°C ≤ T≤ 1000°C

and ρ_{B_4C} will change with the material, FRA or ESK and C_{sup0}=1 for ESK and C_{sup0}=1.4 or 2. for FRA material.

In Fig. 46, we show a comparison between eq. (31) and the experimental results from reference [1] in case of ESK samples.

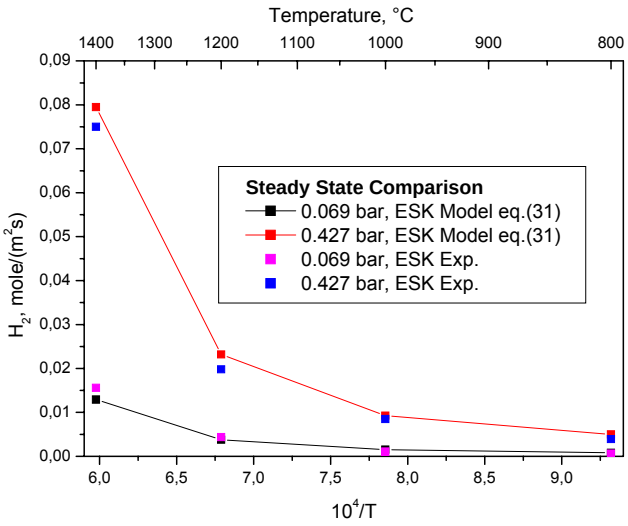

Fig. 46: Comparison between experimental results and the steady state eq. (31) in case of ESK samples.

In Fig. 47, we show a comparison between eq. (31) and the experimental results from reference [1] for FRA samples and C_{sup0}=1.4.

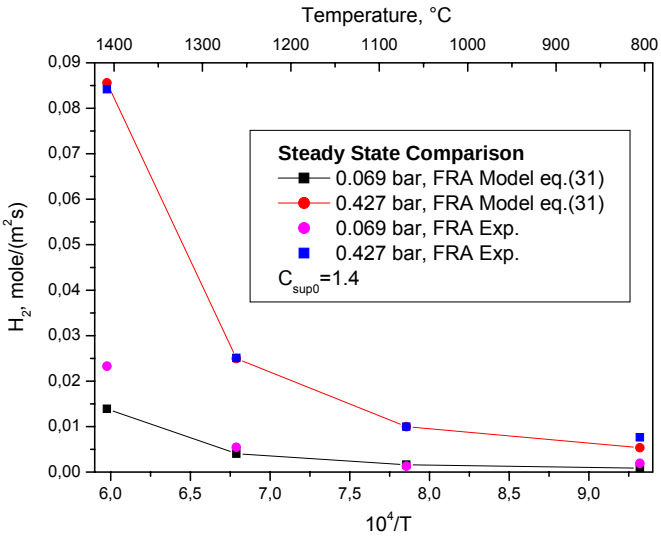

Fig. 47: Comparison between experimental results and the steady state eq. (31) in case of FRA samples, C_{sup0}=1.4.

Because for some FRA samples we use C_{sup0}=1.4 and for others C_{sup0}=2, in Fig. 48, we show a similar result for C_{sup0}=2. In these calculations the model point values are generally bigger than the experimental ones. This could be useful for conservative calculations in accidents codes.

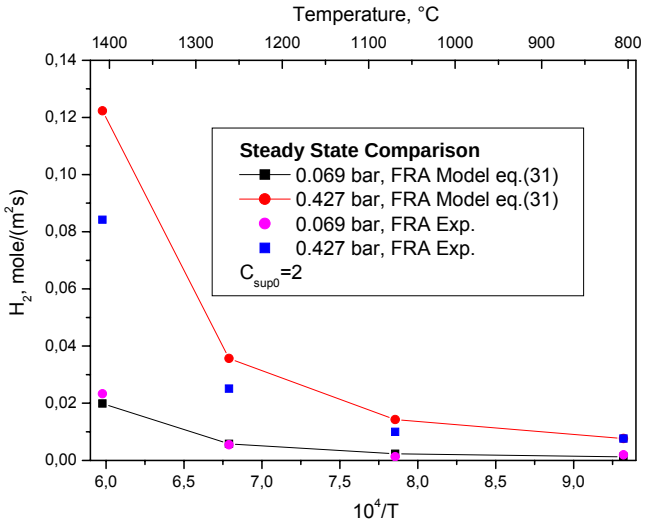

Fig. 48: Comparison between experimental results and eq. (31) in the case of FRA samples, C_{sup0}=2 during steady state.

10.2 The calculation for H_2 generation during temperature transients

We applied the eq. (31) to a transient temperature with C_{sup0}=1.4 according to the previous results. The calculation for H_2 generation during temperature transients, Fig. 49 shows this result. The shape of the resulting peak is similar to experimental test; at 1500°C give a value of 0.164 mole/(m^{2}s) similar to diffusion model, Fig. 41.

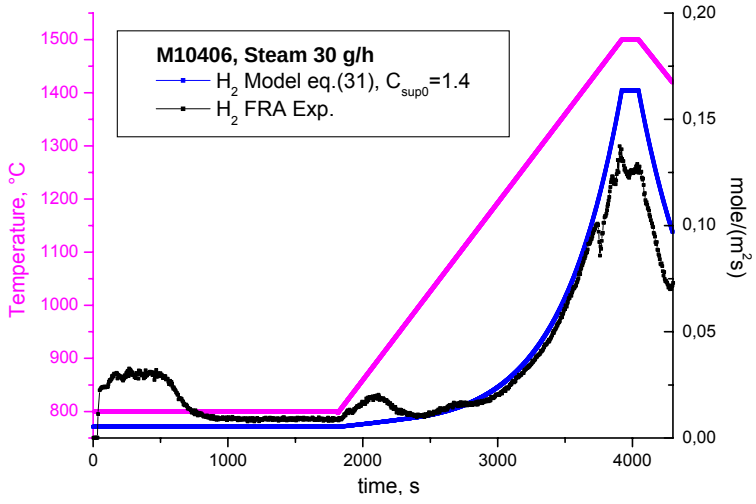

Fig. 49 Transient temperature test with a constant period (0s-1820s) at 800°C and heat up at 1500°C in 2100s, 110s at 1500°C and after cool down at the same speed. The M number corresponds to BOX rig experimental denomination [1].
During a cool-down phase the BOX rig suffers an off-gas pipe blocked at 1420°C.

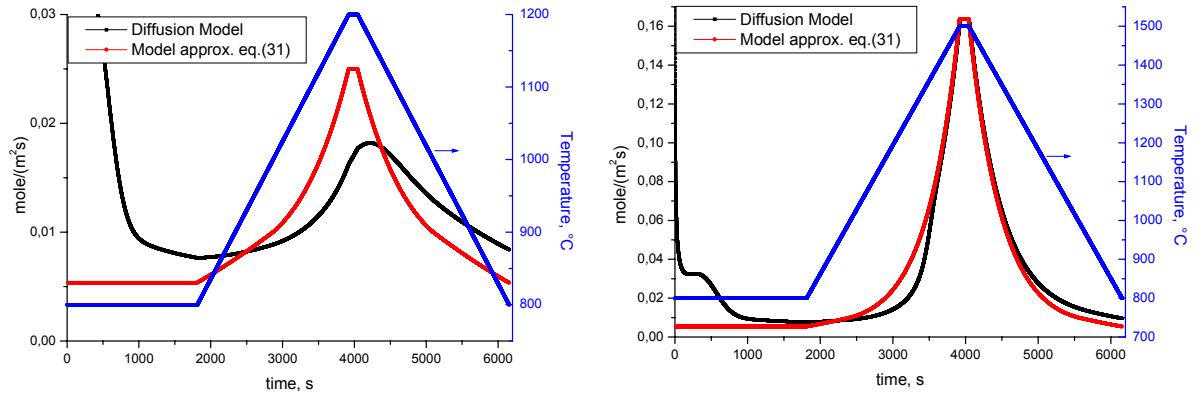

Fig. 50: Comparison between Diffusion Model and eq. (31) for two types of transients. a) The quantity of H_2 from 1800s is H_2(Diff.) = 50.86 mole/m^2, H_2(eq.(31)) = 52.13 mole/m^2. b)The quantity of H_2 from 1800s is H_2(Diff.) = 176.54 mole/m^2, H_2(eq.(31)) = 179.43 mole/m^2.

An off-gas pipe blocked disturbed the experimental result and perhaps this also influences the hydrogen detection at lower temperature. At approximately 1430°C a first perturbation is detected. The result for C_{sub0}=1.4 is acceptable. These results show that the approximation introduced is also good for this type of test where the oxide layer thickness changes simultaneously with the temperature and the steady state condition could never be reached.

As we solve the diffusion equation, we compare the diffusion model calculation, with the approximated eq. (31), during a heat up from 800°C to 1200°C and cool down to 800°C, Fig. 50a, and a heat up from 800°C to 1500°C and cool down to 800°C, Fig. 50b, both at constant steam pressure.

Low temperature has more influence on the gap between Diffusion Model and the eq. (31). Nevertheless, the quantity of hydrogen generated by the peak is equivalent within an error of 2% for these temperature transient speeds. The evolution of the oxide thickness calculated with the diffusion model for the transient of Fig. 50b is showed in the Fig. 51. Nevertheless, the hydrogen generation is nearly constant up to this moment, Fig. 41. After 1812s the heat up starts and the oxide layer thickness reduces the size and rapidly arrives to equilibrium at 1400°C. During cool down the oxide layer thickness increases the size again.

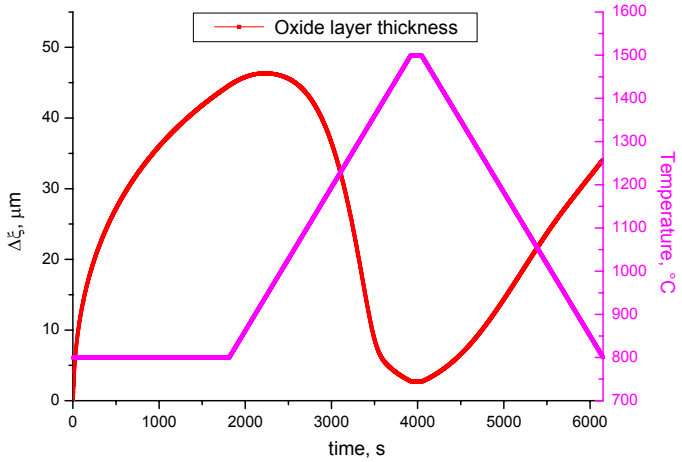

Fig. 51: Oxide layer thickness obtained with a diffusion model as a function of time for the transient of Fig. 50b.

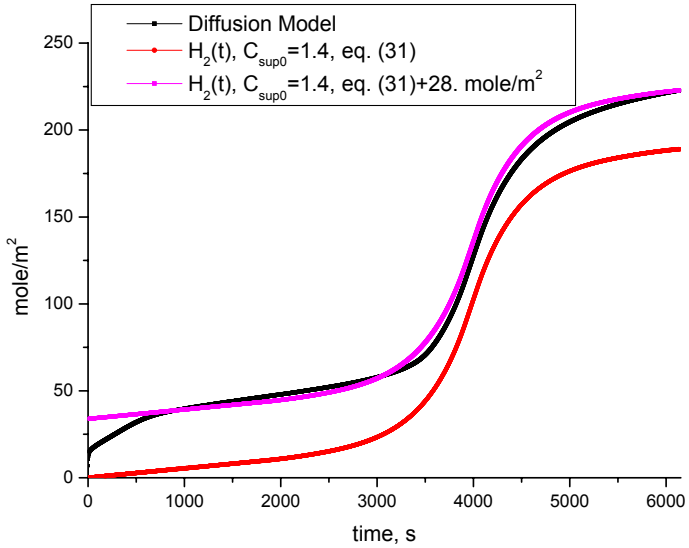

Fig. 52: The total hydrogen generated during a similar transient of Fig. 50b as a function of time.

Diffusion Model with initial peak parameters Fig. 41.

$H_2(t)$, eq. (31)

$H_2(t)$, eq. (31),+ 28. mole/(m^2s) to compare with Diffusion Model.

The calculation is performed with a compressed oxide. The variation of the oxide layer shows that it is not balanced. It is still growing when the temperature starts to increase at 1812s.

Fig. 52, shows that the approximation of eq. (31) is good for the entire transients but fails because it does not include the initial peak. The initial peak is not yet modelled, because of the quantities of experimental points: four temperatures for each steam pressure, Fig. 29, are insufficient to understand its behaviour as a function of temperature. The difference of the two initial peaks under identical experimental conditions is perhaps due to the surface contamination at the beginning of the experiment. The surface cleaning becomes difficult as a consequence of the surface porosity [1,2]. Fig.53, shows a difference of 32%.

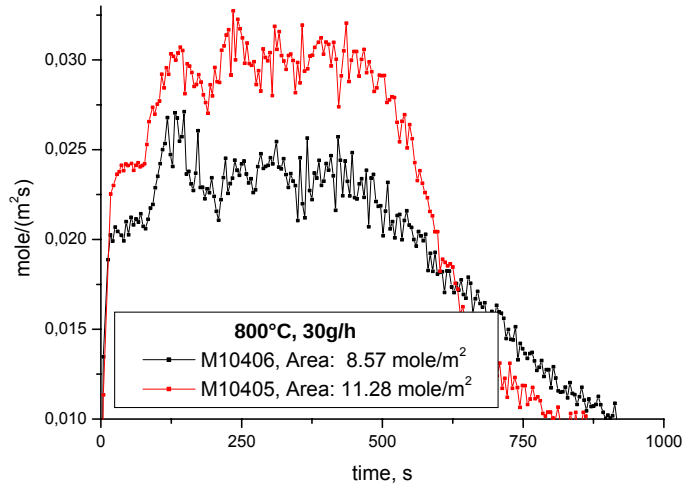

Fig. 53: Two initial hydrogen peaks measured under the same conditions and possibly with different surface contamination in the porosity. The M number corresponds to BOX rig experimental denomination [1].

It is important to notice that an error is introduced in each approximation as it happens for typical correlation in high temperature oxidation of Zry. The approximation of eq. (31) is a correlation for B_4C oxidation in steam, because in this approximation the interaction with air is lost. This correlation introduces errors observable in Fig. 50, more important at low temperature. The difference between the correlation and the diffusion model calculations is evident. A diffusion model like this one was showed before; [8] is the only way to obtain reasonable good results. The diffusion process showed in Fig. 50 could also be represented by a hysteresis loop, if we consider the instantaneous correlation, k_i vs. 1/T, which represents correctly the evolution of the system, instead of the correlation curve to simulate any type of transients. Particularly, in the case of quench simulation process where the temperature change is very quick, the error introduced by any correlation, Cathcart, Pawel's law in the case of Zry and eq. (31) for B_4C, could be very important. An intermediate solution for the big codes could be the use of previously calculated family of hysteresis loops (due to diffusion inertia) with different heat up and cool down speed, Fig. 54. Also in this figure we superpose different transient speeds: -100°C/s, -10°C/s, -2°C/s and 0°C/s from 1500°C. During the transients we change from one loop at constant speed transient to another one according to the instantaneous temperature change. The correlation obtained from equilibrium kinetic curve (0°C/s) could be far from the hysteresis loop (quench trajectory). This last hysteresis loop represents the real evolution of the system.

As an example we show in Fig. 55a, applying to B_4C/steam interaction, we execute the numerical solution of the diffusion proposed model for several constant cool down speeds: -100°C/s, -10°C/s, -1°C/s and 0°C/s from temperature started at 1500°C to 800°C and after keeping constant at 800°C, for oxidation of B_4C at a steam pressure of 0.427 bar, Fig. 55a.

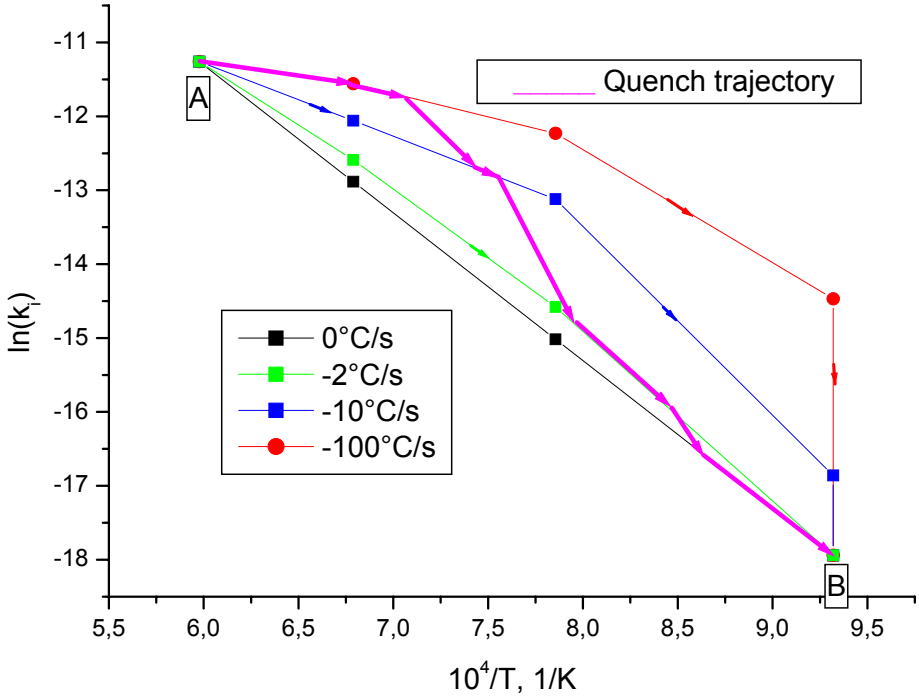

Fig. 54: Schematic representation of a cool down hysteresis loop during quench. The diffusion system quench from high temperature A to low temperature B. The transients start at -100°C/s, changing to -10°C/s to -2°C/s and to 0°C/s (equilibrium correlation).

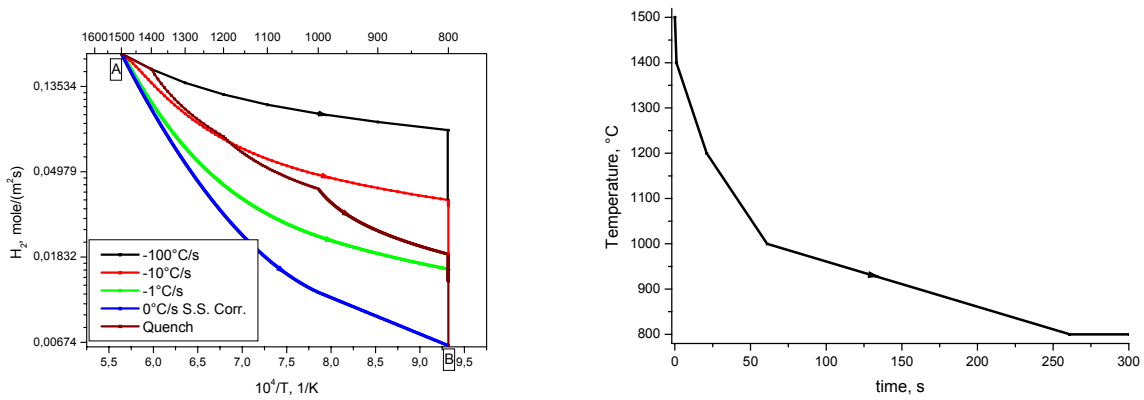

a) b)

Fig. 55: a) Cool down hysteresis loop during quench for different constant cool down speed from –100°C/s to 0 °C/s (steady state correlation). Superposed the oxidation of B_4C during a typical quench temperature vs. time, showed in b).
b) Typical temperature vs. time during quenching: -100°C/s from 1500°C to 1400°C, -10°C/s from 1400°C to 1200°C, -5°C/s from 1200°C to 1000°C, -1°C/s from 1000°C to 800°C and after 0°C/s at 800°C up to reach the equilibrium.

If we superpose a typical B_4C quench oxidation, under the same conditions, corresponding to a curve temperature vs. time showed in Fig. 55b, it is evident that due to diffusion inertia, it is not possible to use the steady state correlation without incurring in an important error especially in the case of quench where the temperature changes very quickly at high temperature. The distance between the correlation equation and the real system path (quench) in Fig. 55a, could be very important. We recommend the use of diffusion solution of the proposed model or in default, the alternative proposed. This means to create a previous diagram similar to the one in Fig. 55a, according to the quench transient plot to build the approximate system path.

10.3 The calculation for H_2 generation during pressure transients

We will now perform a similar comparison in the case of pressure transient, Fig.56. The agreement is good and similar to those obtained in §9.1.3. In all the simulations presented with the eq. (31), the sharp peak does not appear at the beginning of the kinetics, as we expect, because the eq. (31) is only valid for steady state.

The approximation is good under steady state conditions and if the system is keeping at constant temperature including pressure transients. During temperature transients the approximation will have some disagreements depending on the temperature speed and the temperature value. The total hydrogen generated is in good agreement, less than 2 % in the cases of Fig. 50. A complementary equation must be proposed to include in the calculations the contribution of the initial hydrogen peak to the total hydrogen generated during steady state.

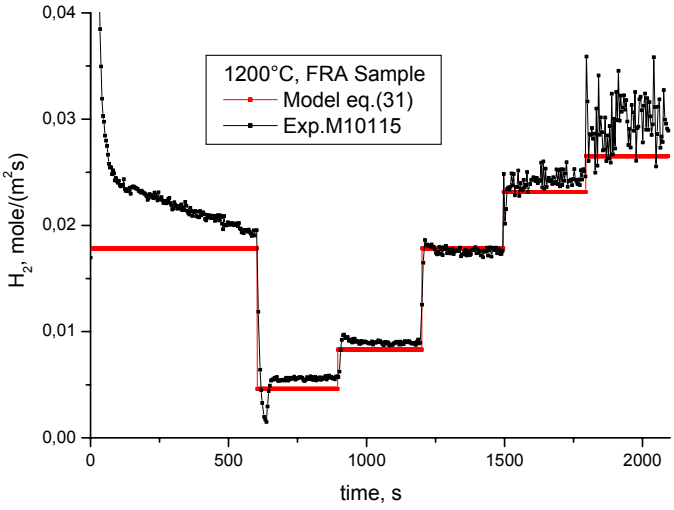

Fig. 56: Pressure transient, comparison between experimental result and eq. (31). C_{sup0}=1.

10.4 The initial hydrogen peak

As mentioned before, the initial hydrogen peak is not yet modelled and the shape and the intensity are perturbed by the contamination of the surface. It becomes difficult to clean the surface because of its porosity. We will propose a calculation based on our previous ideas. When the oxide layer is small, the time necessary to cover with liquid B_2O_3 the surface of the sample is bigger and the signal intensity of the initial hydrogen peak is also bigger. That is why we will use the approach of Fig. 36, improved in order to adjust the values to those of Fig.36b.

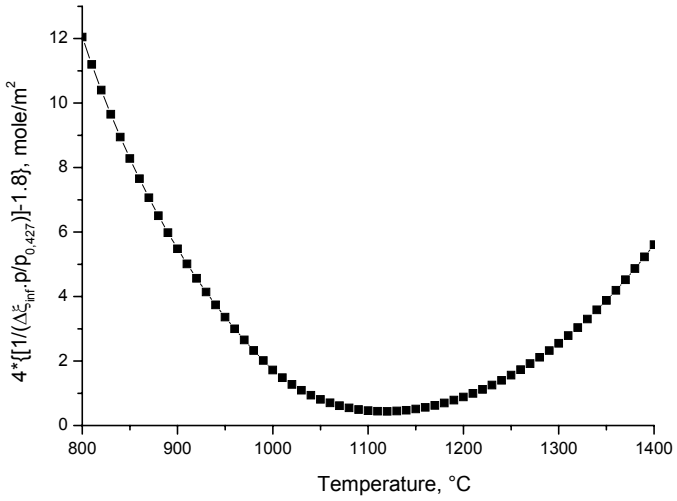

Fig. 57: The intensity of initial hydrogen peak as a function of temperature.

The equation proposed for the initial hydrogen peak related with the oxide layer thickness is, Fig. 57:

$$H_{Initial-peak} = 4 * (\frac{1}{\Delta\xi_{t=\infty} \frac{p}{p_0}} - 1.8)$$

It has approximately the form and the values of the Fig. 36b. To all the calculations of the initial hydrogen peak it is necessary to add the very sharp peak generated during the first seconds and which corresponds to 6 - 10 mole/m^2. It clearly appears in Fig. 41, H_2 calculated by the diffusion model.

11. Discussion

The analysis of the BOX rig experimental results shows that the evolution of each of the species has not the same behaviour. We assume that it is due to the different origins of each non-condensable species: the external surface of boron oxide or the interface between the boron oxide and the boron carbide. This allows us to propose an oxygen diffusion model through the boron oxide. However, several questions about an important number of hypotheses announced remain without any answer. New experimental results to confirm that hypothesis would be necessary. For example the oxidation of boron carbide under Argon+Oxygen atmosphere (air simulation) would perhaps inform us about the Carbon behaviour in the boron oxide discussed in §4.1. It would also be interesting to know how the generation of CO_2 and CO could be modified by the absence of water. The TG test shows that the oxidation in Argon + Oxygen is possible to be simulated with the same proposed model and operating very small changes in only one variable. Therefore, under these new conditions (Argon Oxygen) the CO_2 and CO could also show different kinetics in comparison with Ar+Steam atmosphere.

From now on, this proposed model has several parameters with upper and lower limits like the oxygen diffusion coefficient or C_1 that is constant for the whole BOX rig test but it is not justified yet. Of course D_O and C_1 have complementary incidence on the oxide layer thickness during steady state. The surface porosity has not a model up to now, only a simulation equation. Hydrogen generated during the initial peak is only important for very shorts kinetics.

Quench process is always related with very rapid changes in temperature. Therefore the use of correlation equations will introduce important errors in the calculation of oxide layer thickness and gases generated during the quench transients. The best solution is the use of diffusion equations to solve the interaction problem or applied an intermediately troubleshooting like we propose here, §10.2.

12. Conclusions

The model proposed seems to be a good one to simulate both the BOX rig test and the Thermogravimetric test. It consists in an oxide layer of liquid boron oxide that controls the oxygen diffused from the external oxide surface to the interface “boron oxide/boron carbide” to oxidize the boron carbide together with a superficial reaction between the liquid boron oxide and steam or air. For the Thermogravimetric test it is performed in Argon+Steam and in Argon+Oxygen atmospheres when the steam pressure is zero, all in a temperature range 800°C to 1400°C. We show from the evolution analysis of non-condensable (H_2, CO_2, CO and CH_4) gases the different origins of each species. In the “steam/liquid boron oxide” interface I_1, the H_2 is generated from water dissociation with the necessary oxygen quantity to oxidize after diffusion in the liquid boron oxide the B_4C and a part of C to CO in interface I_2 “liquid boron oxide/ boron carbide”. The CO_2 is also generated in interface I_1 oxidizing the carbon dissolving in the liquid boron oxide. In the “liquid boron oxide/boron carbide” interface I_2 the CO already mentioned and CH_4 are generated. The superficial reaction in the interface “steam/liquid boron oxide” produces the boric acids and directs B_2O_3 evaporation. The superficial reaction is dependent on temperature and steam pressure, but not on argon carrier speed in the range of 10 to 100 l/h.

As the calculation of diffusion equation involves extra computing time we propose a simplified equation particularly useful for big codes in the case of interaction between boron carbide and steam during quench process.

The proposed model is able to simulate the non condensable and the total condensable gases generation in the case of BOX rig test under Ar+Steam atmosphere during different experimental conditions like isothermal tests, transient temperature tests and transient steam pressure tests or in the case of thermogravimetric experiments under Ar+Steam and under $Ar+O_2$ (air simulation) atmosphere in different isothermal conditions. It is also possible to switch during any of these kinetics, Ar+Steam or $Ar+O_2$, to inert atmosphere and the system will freeze some time later when the equilibrium will be reached.

13. Acknowledgements

The author is very grateful to Dr. Martin Steinbrück, IMF I, for the invitation to participate into his research group and to Dr. Delia Mata-Ciampoli for reviewing this manuscript.

14. References

1) M. Steinbrück, A. Maier, U. Stegmaier, L. Steinbock, Experiments on the Oxidation of Boron Carbide at High Temperatures, Report FZKA 6979, Karlsruhe, 2004.

2) W. Krauss, G. Schanz, H. Steiner. “TG-Rig Test (Termal Balance) on the Oxidation of B4C, Basic Experiments, Modelling and Evaluation Approach“. SAM-COLOSS-P027, FZKA 6883, Karlsruhe, 2003.

3) M. Steinbrück, W. Krauss, G. Schanz, H. Steiner, A. V. Berdyshev, M. S. Veshchunov. Unpublished report, Forschungszentrum Karlsruhe, 2003.

4) L. N. Efimenko, E. V. Lifshits, I. T. Ostapenko, I. A. Snezhko and É. P. Shevyakova, Sov. Powder Metall. Met. Ceram. 27 [1987] 318/21.

5) Gmelin Handbook, B 4th Suppl. Vol. 2, p.19

6) L. Belovsky, IAEA TCM on “Behavior of LWR Core Material under Accident Conditions”. October 9-13, 1995, Dimitrovgrad, Russia.

7) E. A. García and J. Kovacs, Journal of Nuclear Materials 210 (1994) 78-83.

8) E. A. García. "Diffusion Processes in Nuclear Materials under Accidental Conditions", pag.: 391-420. Chapter of book: "Diffusion Processes in Nuclear Materials". Editor R.P.Agarwala. Elsevier Science Publishers B.V., The Netherlands. 1992.